# INVESTIGATION ON ELECTROCATALYTIC BEHAVIOUR OF SOL-GEL DERIVED CuO/PANI NANOCOMPOSITE

A Major Project Submitted In the Partial Fulfillment of the Requirement

For the Award of the degree of

**MASTER OF TECHNOLOGY**

**IN**

**POLYMER TECHNOLOGY**

Under the Supervision of

**Prof. D.KUMAR**

(Project Guide & Head)

Department of Applied Chemistry

& Polymer Technology

Delhi Technological University

Delhi - 110042

BY

ALKESH KUMARI

(2K12/PTE/01)

DEPARTMENT OF APPLIED CHEMISTRY & POLYMER TECHNOLOGY

DELHI TECHNOLOGICAL UNIVERSITY, DELHI- 110042

**DELHI TECHNOLOGICAL UNIVERSITY**

**(Govt. of National Capital Territory of Delhi)**

**Shahbad Daulatpur, Main Bawana Road,**

**Delhi - 110042**

# CERTIFICATE

This is to certify that Ms. Alkesh Kumari has Satisfactorily Completed this Major project entitled "**Investigation on electrocatalytic behaviour of sol-gel derived CuO/PANI nanocomposite**" in the Partial Fulfillment for the Award of the Degree of Master of Technology in Polymer Technology of Delhi Technological University, Delhi During the academic Session 2013-14.

To the Best of my knowledge and Belief, this Work has not been submitted to any other University or Institutions for the Award of any Degree or Diploma.

**Prof. D. Kumar**

Project Guide & Head

Department of Applied Chemistry &

Polymer Technology,

DTU, Delhi-110042

# ACKNOWLEDGEMENT

Taking the opportunity of this column, I would like to express my sincere gratitude to all those who directly or indirectly helped me in successful completion of my project.

First of all I heartedly express my humble gratitude to **Prof. D.KUMAR**, Department of Applied Chemistry & Polymer Technology, Delhi Technological University (Formerly Delhi College of Engineering), for providing me the facilities, guidance, suggestions and constant encouragement throughout the tenure of my project work. I am deeply indebted to him for giving me an opportunity to work with him and helping me in every possible way in bringing out this work to reality.

I also would like to express any sincere gratitude to **Dr. Jay Singh**, Department of Applied Chemistry & Polymer Technology, Delhi Technological University (Formerly Delhi College of Engineering), complete my entire project under their valuable guidance, constant support, encouragements and many insightful conversations and helpful discussion which made this thesis possible.

I am also thankful to Dr. Sameer Sapra, Professor Department of Chemistry, Indian Institute of Technology, Delhi, for his kind assistance for providing XRD spectra.

I like to express my sincere thanks to Department of Anatomy, All India Institute of Medical Sciences, New Delhi, for providing TEM spectra for my Metal oxide samples.

I am very much thankful to Department of Biotechnology for providing antibacterial study.

I am grateful to all the staff members of the Department of Applied Chemistry and Polymer Technology (Formerly Delhi College of Engineering), Delhi Technological University for their kind help in various occasions in my Project work.

I would like to continue by thanking Ms. Reetu Prabhakar, Ms. Sarita S.Nair, Ms. Nidhi, Mr. Vinay, Mr. Ratnesh , Mr. A. V. Ullas, (research scholars), Mr. Sandeep Mishra and Mr. Aman Verma (Technical assistant) for their massive help in making me understand the basics of techniques and patiently responding to my incessant doubts.

I am thankful to all laboratory staff and colleagues for their co-operation.

I wish to thank my friends Priya Malik and Manish Kumar for their motivation and cooperation all throughout.

Last, but not the least, my parents, my brothers, my husband and my well-wishers have been with me at every step of this exciting journey. I thank them for all their prayers, encouragements and best wishes.

Date:

***Alkesh Kumari***

**2K12/PTE/01**

# UNDERTAKING

I, Alkesh Kumari, hereby declare that the work entitled "Investivation on electrocatalytic behaviour of sol-gel derived CuO/PANI nanocomposite" has been carried out by me under the guidance of Prof. D. Kumar, Delhi Technological University, Delhi.

This dissertation is part of partial fulfilment of requirement for the degree of M. Tech in Polymer Technology. This is the original; work and has not been submitted for any other degree in any other university.

Date:
Place: DTU, Delhi

Signature of the candidate

# CONTENTS

# LIST OF TABLE

## S. No Caption

# LIST OF FIGURE

# ABSTRACT

In this project report, I tried to present results of the studies related to fabrication of a metal oxide based efficient non-enzymatic sensor using an interface based on sol-gel derived nanostructured copper oxide (CuO). A colloidal solution of prepared nanostructures has been electrophoretically deposited (EPD) onto an indium-tin-oxide (ITO) glass substrate. The structural and morphological studies of CuO nanostructures have been carried out by X-ray diffraction (XRD) (particle size 7-8 nm) , UV-visible spectroscopy (UV-Vis), photoluminescence spectroscopy (PL) and Fourier transform infrared (FTIR) spectroscopic techniques scanning electron microscopy (SEM), transmission electron microscopy (TEM), atomic force microscopy (AFM). Polyaniline (a conducting polymer) was ultrasonically prepared and used as a matrix to prepare the nanocomposite. The CuO nanostructures were then ultrasonically dispersed in Polyaniline (PANI) solution, and then used to form CuO/PANI nanocomposite film by electrophoretic deposition method on the ITO plate. The CuO/PANI/ITO nanocomposite film was found to provide improved sensing characteristics to the electrode interface in terms of electroactive surface area, diffusion coefficient, charge transfer rate constant and electron transfer kinetics. This interfacial platform has been used for fabrication of a non-enzymatic sensor for $H_2O_2$ sensing. The results of response studies of the fabricated CuO/PANI/ITO electrode show a linear range of 2-22 mM, detection limit of 20.7 mM, and high sensitivity of $0.0317 \mu M cm^{-2}$ with a response time of 20 s. The utilization of this CuO modified electrode for electo-oxidation of $H_2O_2$ offers an efficient strategy and a novel interface for application of tin oxide in the field of electrochemical sensors.

# 1 INTRODUCTION

## 1.1 Nanotechnology

Nanotechnology and nanoscience are the study and application of highly small matters and can be used over all the other science fields, for example materials science, chemistry, physics, biology and engineering [1]. National nanotechnology initiative demonstrated a more generalized description of nanotechnology, which determines nanotechnology as the use of matter with at least one dimension sized from 1 to 100 nm [2]. Technology carried on nanoscale (nm) so called nanotechnology. Physicist Richard Feynman is the father of nanotechnology. All things on earth are made up of atoms – the buildings and houses we live in, the food we eat, the clothes we wear and our own bodies. Nanotechnology requires the ability to see atoms and molecules. But sometimes atom is not possible to see by naked eye. So there are many important advanced developments launched such as atomic force microscope (AFM), scanning tunnelling microscope (STM), scanning electron microscope (SEM), transmission electron microscope (TEM) etc. The atomic force microscope (AFM) and the scanning tunnelling microscope (STM) are two former interpretations of scanning probes that founded nanotechnology [3,4].

Today's engineers and scientists discovering a broad variety of ways to purposely make material at the nanoscale. They obtained advantage by raised properties like strength, lighter weight, greater chemical reactivity, enhanced control of light spectrum. Scientists currently argue the future significances of nanotechnology. Nanotechnology may be capable to produce many new materials and devices with a huge range of applications, such as in medicine, energy production, electronics and biomaterials [5]. Second is nanotechnology bringing up many of the same effects about the toxicity and environmental affect of nonmaterial's and their potential issues on global economics.

## 1.2 Nanostructural material (Metal oxide)

In the periodic table great number of transition metals is present and these metals have a several applications in unlike fields. These transition metals have oxides in nature but in day to day life some of the metal oxides are utile in science and technological applications. These metal oxides are a significant class of semiconductors, which have several applications such as solar energy transformation, magnetic storage media, electronics and catalysis [6-14]. Among the transition metal's oxides, CuO is a semiconductor that is being studied widely because of its concerning properties and applications. Semiconductor are interesting materials because of their large practical importance in optoelectronic and electronic devices, such as magnetic storage devices [15], electrochemical cell [16], high Tc super conductors [17], gas sensors [18], nanofluid [19], field emitters [20] and catalysts [21].

CuO has categorised in p-type of semiconductors and has awesome properties such as physical, electrical, magnetic and optical. Some transition metal monoxides such as MnO, FeO, CoO, NiO and CuO are antiferromagnetic in nature. MnO, FeO, CoO and NiO belong to NaCl structure system but the CuO has a monoclinic structure [22]. The antiferromagnetic behaviour of CuO is due to the exchange interaction between $Cu^{+2}$ ions via $O^{-2}$ ions. In monoclinic unit cell, the lattice parameters for CuO are a=4.6837Å, b=3.4226Å c=5.1288Å, α=90º, β=99.54º and γ=90º. In the structure copper ions is coordinated by 4 oxygen ions and has approximately square planar configuration [23].

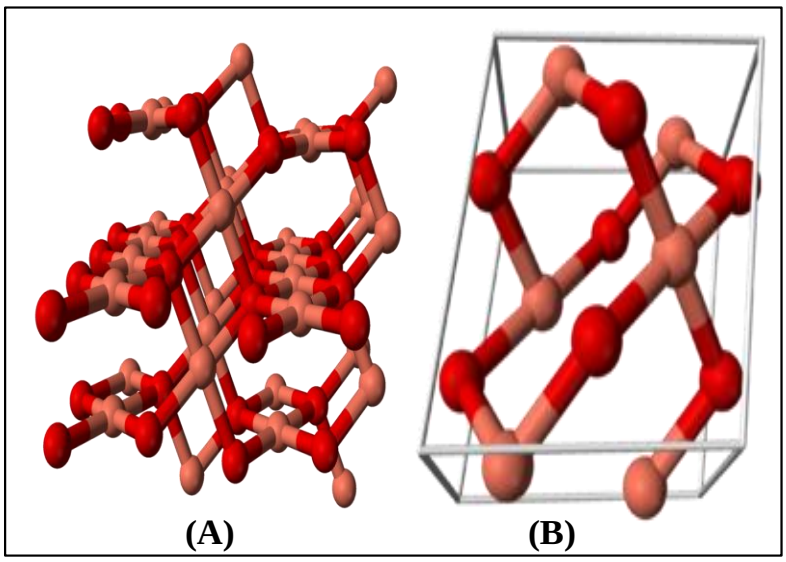


**Fig. 1.1:** (A) Crystal structure of CuO (B) The unit cell CuO

All metal oxide is not show catalytic activity but CuO acts as a catalyst due to their potentiality. CuO has high activity and selectivity in oxidation/reduction reactions so it used as a catalyst. CuO also used in the synthesis of higher alcohols and methanol. It completely convert hydrocarbon into $CO_2$, water shift and steam reforming of low molecular weight alcohols and oxidation of organic and organosulfur compounds [24-28].

CuO are used as an active and passive component in many applications like-gas sensor [18], magnetic storage media [15], batteries, semiconductors, heterogeneous catalysis [21], solar energy conversion, photovoltaic and field emission due to exhibiting small band gap of 1.2 eV. CuO nanostructure is prepared in various shapes like nanorod, nanobelts, nanoparticles, nanoplatelets, nanowire, nanoflower and nanoneedle [29-31].

There are wide variety of methods for synthesis of nanoparticles but we select one, i.e., widely used and more preferable. There is number of preparation methods are available for synthesis of CuO nanoparticles. Various methods like thermal oxidation, sol-gel, hydrothermal, solvothermal, electrodeposition, combustion, alkoxide based synthesis sonochemical, solid-state reaction, thermal decomposition, microwave irradiation and precipitation. Among these methods our preparation method for the synthesis of CuO nanoparticles belongs to chemical method, i.e., sol-gel method and particle size obtained 7-8 nm. The range of the particles from the preparation methods as fallows in case of sonochemical method is around 10 nm to several microns [32]. MOCVD (metal organic chemical vapour deposition) CuO nanoparticles is 0.05 to 8 μm [33]. Some results shows in some references which is in the range of 1-10 nm nanoparticles in sol-gel method [34]. The average diameter of the CuO nanoparticles in solid state reaction is given by 15-20 nm [35]. Smallest CuO nanoparticles were prepared by electro chemical method and size is around 4 nm [36].

## 1.3 Polyaniline (PANI)

PANI is the virtually useful within the family of conjugated polymers because of air and moisture-stable in its doped, de-doped, conducting form and insulating form [37-39]. PANI has very simple doping/dedoping, acid/base chemistry and has various potential applications such as anticorrosion coating, antistatic coatings, batteries, separation membranes and sensors [40.41].

In chemical polymerisation reaction nanostructures of PANI (diameters lower than 100 nm) have been formulated by inserting structural directing agents such as surfactants [42-45], polyelectrolyte's [46], aniline oligmers [47], liquid crystals [48], nanowire seeds [49] and bulky organic dopants [50-54].

### *1.3.1: Synthesis and properties*

PANI is most studied conducting polymer and has semi-flexible rod property. It has charismastic processing properties within organic semiconductors and family of conducting polymers due to chemistry. Polymerized from cheap aniline monomer, PANI has three idealized oxidation states:

(1) Leucoemeraldine – white /clear & colourless $(C_6H_4NH)_n$

(2) Emeraldine – green for the emeraldine salt, blue for the emeraldine base $([C_6H_4NH]_2[C_6H_4N]_2)_n$

(3) (Per) nigraniline - blue/violet $(C_6H_4N)_n$

Leucoemeraldine is fully reduced state with amine links, pernigraniline is fully oxidized state, have imines links and the emeraldine form is neutral and concerned to as emeraldine base (EB). During doping process, acid give proton to imines nitrogen so it is called emeraldine salt. Diiminoquinone-diaminobenzene state are delocalize after protonation. Emeraldine base is considered as the most useful form of PANI due to doping high stability at room temperature. Leucoemeraldine and pernigraniline form of PANI are lower electrically conducting but emeraldine salt form are highly electrically conducting on doping with an acid [38].

In different oxidation states, PANI show colour change that's can be applied in sensors and electrochromic devices. Different oxidation states or doping levels are changes in electrical conductivity during PANI synthesis. Treatment of emeraldine with acids enhances the electrical conductivity by ten orders of magnitude.

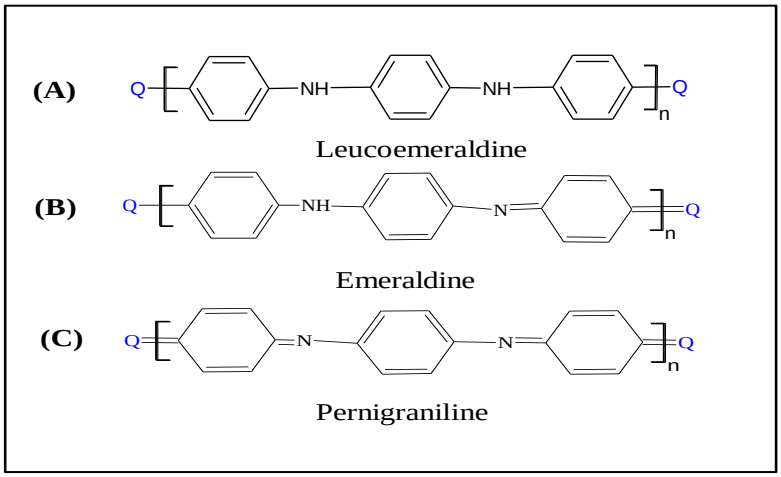


**Fig. 1.2:** Oxidation states of polyaniline-(A) Leucoemeraldine (B) Emeraldine (C) Pernigraniline

***Synthesis***

Although the synthetic methods to produce PANI are quite simple, the mechanism of polymerization is probably complex. The formation of leucoemeraldine can be described as follows, where [O] is a generic oxidant.

$$nC_6H_5NH_2 + [O] \rightarrow [C_6H_4NH]n + H_2O$$

The most common oxidant ammonium persulfate. The components are each dissolved in 1M hydrochloric acid (other acids can be used), and the two solutions slowly combined. The reaction is very exothermic. The polymer precipitates as an unstable dispersion with μm scale particulates.

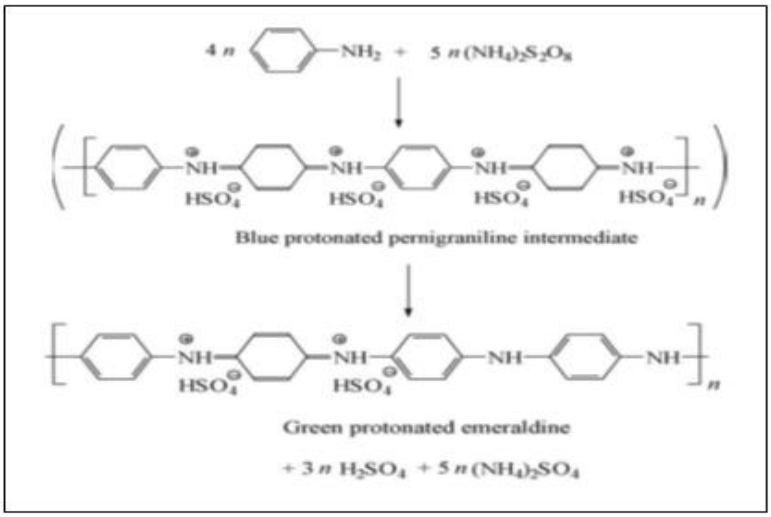


**Figure 1.3**: Synthesis of emeraldine form of PANI

During the reaction oxidation of aniline with ammonium persulfate in acidic medium yields the emeraldine form of PANI. A protonated pernigraniline is an intermediate. Sulphuric acid and ammonium sulphate are by-products [37, 38].

There are wide variety of methods for synthesis of polyaniline nanoparticles such as chemical method (conventional method), interfacial method, ultrasonic method etc but we select one , i.e., give uniformly particle size and better result than others. We used ultrasonic method for polyaniline synthesis. Now days ultrasonic method is an advanced technique that is widely used for synthesis of nanoparticles.

### *1.3.2: Applications*

PANI and the other conducting polymers such as, polythiophene, polypyrrole and PEDOT/PSS have potential for applications due to their light weight, conductivity, mechanical flexibility and low cost. PANI is especially attractive because it is relatively inexpensive, has three distinct oxidation states with different colours and has an acid/base doping response. This latter property makes polyaniline an attractive for acid/base chemical vapour sensors, supercapacitors and biosensors. The different colors, charges and conformations of the multiple oxidation states also make the material promising for applications such as actuators, supercapacitors and electrochromic. They are suitable for manufacture of electrically conducting yarms, antistatic coatings, electromagnetic shielding, and flexible electrodes [40].

Attractive fields for current and potential utilization of PANI antistatics, charge dissipation or electrostatic dispersive (ESD) coatings and electromagnetic interference shielding (EMI), anti-corrosive coatings, hole injection layers, transparent conductors, ITO replacements, actuators, chemical vapor and solution based sensors, electrochromic coatings (for colour change windows, mirrors etc.), PEDOT-PSS replacements, toxic metal recovery, catalysis, fuel cells and active electronic components such as for non-volatile memory. Among the family of conjugated polymers, PANI is one of the most useful since it is air- and moisture-stable in both its doped, conducting form and in its de-doped, insulating form. PANI is also unique among conducting polymers in that it has a very simple acid/base doping/dedoping chemistry. Currently, the major applications are printed circuit board manufacturing (final finishes, used in millions of $m^2$ every year), antistatic and ESD coatings, and corrosion protection [41].

## 1.4 Metal oxide/Polymer nanocomposites

Nanocomposites are special class of materials having unique properties and wide applications potential in different areas. The polymer nanocomposites have attracted great interest owing to their novel properties derived from the successful combination of the characteristics of parent constituent into a single material. The unparallel advantage such as cost-effective process ability, lightweight and tuneable mechanical, electrical and optical properties for the diverse application such as microwave absorption layers, gas sensors, super capacitors.

The aim of nanocomposite preparation is find the synergic effect of the inorganic compound and the polymer. Nanocomposites have a particular structure that is called phase differentiated structure. There is a nanoscale interface present between the polymer and inorganic compound. This phase differentiated structure act as an important characteristic in the production of a molecular-charge synergic effect between the polymer and inorganic compounds in nanocomposites (Paul and Robeson 2008).

Nanocomposite with a phase differentiated structure in nanoscale can be developed by 4 dissimilar methods: (1) Implanting an inorganic moiety into the polymer. (2) Using diffusing polymer networks with chemical bonds, (3) integrating inorganic groups by bonding them to the polymer backbone and (4) organizing a dual inorganic-organic hybrid polymer (Kickelbick 2003). Many kind of synthesis processes have been suggested such as sol-gel process (chemical process), facial synthesis, core-shel composite and electrophoretic deposition. Among these synthesis processes we prepare CuO/PANI nanocomposite by electrophoretic deposition (EPD) method.

The nanocomposites of conducting polymers with inorganic semiconducting nanomaterials show the improved mechanical, electrical and thermal properties due to the combined effects of both the semiconducting nanomaterials and conducting polymers. In particular, PANI nanocomposites display applications on a large scale for various electrochemical, electrorheological and in the electronic fields such as batteries, sensors, controlling systems and organic displays.

As one of the important metal oxides, CuO is frequently used as anode materials for LIBs owing to its high capacity, environmental benignity, safety and low-cost Therefore, the preparation of composite of PANI and metal oxide becomes a novel challenge for people.

EPD is the deposition of thin films of nanocomposite and nanomaterials on the conducting electrode surface for the manufacturing of electrochemical transducers. Within these syntheses EPD technique is experienced to yield uniform, dumb and porous films with advantages of reduced processing time and simple experimental design. EPD allows for easily control of thickness and morphology of the deposited film depends on applied potential, deposition time etc [55-56]. Electrophoretic deposition (EPD) is one of the convenient methods that develop such coating. During the EPD process, when electric field applied then charge particle in aqueous are moved to oppositely charge electrode and deposited onto electrode [57]. In EPD process, uniform particle packing depends on the amount of surfactant, conductivity, concentration and pH [58]. EPD has advantage because it provides the possible action of coating substrates of composite shape, exact control of coating thickness, and required elementary equipment. Combining of polymers and metal oxide can be used to form organic-inorganic soft composite coatings. These composite coatings can detect various applications in industrial sectors and medicine. In medical sector soft composite coatings allow for best connection between fixed metallic implants and vascularise bone tissue [59,60].

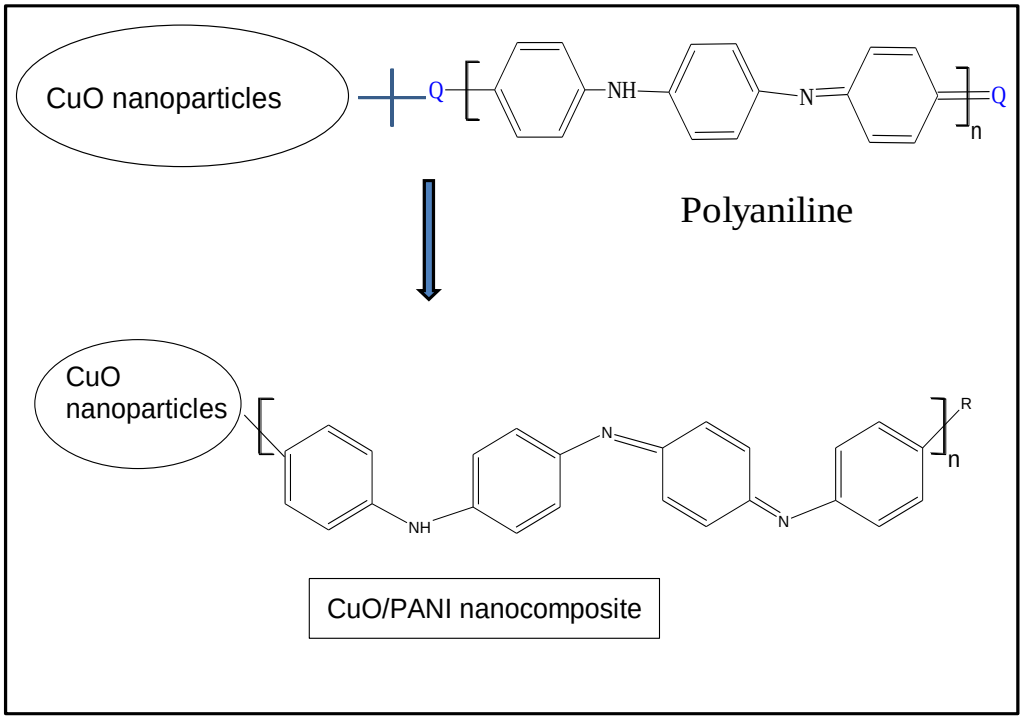


**Fig.1.4:** Schematic picture of CuO/PANI nanocomposite synthesis

Now days, polymers with particular functional groups are applied as particular stabilizers for the synthesis of nanocomposite having various properties. Polymer based nanocomposite have unique features when compared to other bulk materials. Within the family of conducting polymers, for the past 20 years PANI is the virtually studied conducting polymer because of its facial synthesis [61]. PANI have awesome electronic properties, chemical and environmental stability and semiconducting nature so it produce nanocomposite with inorganic metal oxide. We have synthesized monodispersed CuO nanoparticles mixed with polyaniline matrix using EPD onto the glass substrate. The combination of PANI with CuO is used as substitute materials for optoelectronic applications. Luminescence from the polyaniline implanted CuO nanoparticles is highly enhanced and improve stability is obtained from the nanocomposites. Photoluminescence (PL) is significant technique for detecting the energy gap, crystalline quality detects purity and analysis the quantum labour of the materials [62].

***Metal oxide/Polyaniline nanocomposites***

Subhash Kondawar et al have been synthesized Cadmium Oxide Nanoparticles Embedded PANI Nanocomposites and compare its conductivity to pure PANI and Cadium oxide nanoparticles. The synthesized nanocomposites were subjected for spectroscopic and structural characterization using FTIR, UV-VIS and SEM, XRD respectively. Nanocomposites show high electrical conductivity compared to pure PANI. The conductivity of nanocomposites increases with increasing of CdO content because of the new conductivity passageways formed by embedded nanoparticles of CdO.

Feng-Yi Chuang, et al have been prepared Titanium Oxide and PANI Core-Shell Nanocomposites. The composites were characterized by FTIR, ESCA and TEM. FTIR spectra. The shape of the particles in the composite is spherical which is different from that of titanium oxide crystal and fibular structure of PANI polymerized under the same condition.

A.A. Matnishyan et al discussed the synthesis of a nanosized highly conductive PANI composite with tin and titanium oxides have been proposed. The morphology, composition, IR spectra, conductivity, and thermal stability of the synthesized samples have been studied.

***CuO/Polymer nanocomposite nanocomposite***

Zhanhu Guo et al synthesized CuO nanoparticles filled vinyl-ester resin nanocomposites. Thermal degradation study by thermo-gravimetric analysis (TGA) showed the increased thermo-stability in the functionalized-nanoparticles-filled vinyl-ester resin nanocomposites as compared with the unmodified-nanoparticles-filled counterparts.

Zhigang Yin et al have described the synthesis of One-dimensional core–shell CuO/polypyrrole (PPy) nanocomposites by employing CuO nanobelts When evaluated as potential anode materials for lithium-ion batteries, the novel CuO/PPy nanocomposites exhibit a high initial capacity of 991 mAh $g^{-1}$ and retain a good reversible value of 613 mAh $g^{-1}$ over 80 cycles, which are much better than those of the bare CuO nanobelts.

M Gouda et al have fabricated CuO/Chitosan Nanocomposite for Antibacterial Finishing Cotton Fabric. Cotton fabric treated with CuO/Chitosan nanocomposite was characterized via scanning electron microscope supplied with energy dispersive spectroscopy to verify the elemental composition of deposited materials on the fabric. Antimicrobial activity of the prepared fabric samples treated with chitosan nanoparticles and CuO/chitosan nanocomposites against Gram +ve bacteria (*Staphylococcus aurous*) and Gram -ve bacteria (*Escherichia coli*) were investigated. Durability of treated cotton fabrics with nanocomposites has been evaluated.

In this project, CuO/PANI/ITO electrode synthesized through the appropriate addition of CuO nanostructures and PANI and electrophoretically deposited onto ITO electrode. The prepared electrode has been characterized by SEM, AFM, FTIR, UV, XRD, PL, and electrochemical techniques for enhances electrocatalytic properties of $H_2O_2$. This work provides an easy going and effective route for the synthesis of CuO/PANI nanocomposite.

## 1.5 Objective and methodology

***Objective***

For the fabrication of CuO/PANI nanocomposite electrode for Electro-oxidation study of Hydrogen peroxide following experiments have been conducted:

(i) Synthesis of the Copper oxide (CuO) nanostructure by sol-gel method.
(ii) Particle size distribution and crystal size calculation of these nanoparticles through TEM and XRD.
(iii) Preparation of thin film electrodes using various deposition techniques like electrochemical deposition, electrophoretic deposition (EPD).
(iv) Preparation of polymer solution and polymer based metal oxide nanocomposite film.
(v) Fabrication of CuO/PANI nanocomposite film electrode for sensing of hydrogen peroxide.
(vi) Surface morphological studies and element analysis of the metal oxide based film electrodes using SEM, EDX and AFM.
(vii) Bonding characteristics of these fabricated electrodes through FTIR studies.
(viii) Amperometric measurements and electrochemical characterization like CV, DPV of these fabricated electrodes using potentiostat/galvanostat instrument.
(ix) Electrochemical response studies of the bioelectrodes using sensing parameter like linearity, sensitivity, low detection limit, linear regression, and standard deviation.
(x) Other electrochemical studies like effect of potential, pH, response time.

***Methodology adopted to achieve the above objective:***

To achieve the above objectives, we plan to follow the methodology described below**:**

(i) Synthesis of the CuO nanostructure using sol-gel method.
(ii) Structure and crystal size calculation of CuO nanostructure through XRD.
(iii) Preparation of CuO/PANI nanocomposite film on ITO by electrophoretic deposition. The CuO nanostructure and PANI were dispersed in double DI water followed by ultrasonication.

(iv) EPD for CuO/PANI nanocomposite electrodes fabrication.

(v) Surface morphological studies and element analysis of the electrodes using SEM, EDX.

(vi) Bonding characteristics of those fabricated electrodes through FTIR.

(vii) Amperometric measurement and electrochemical characterization like CV, and DPV.

(viii) Electrochemical response studies of the nanocomposite electrodes using sensing parameter like linearity, sensitivity, low detection limit, linear regression, and standard deviation.

(ix) Investigation of the effect of potential, pH, response time, stability on the fabricated nanocomposite electrode.

(x) Application of prepared nanocomposite electrode for Hydrogen peroxide sensing.

## 2 Experimental work and Characterisation

### 2.1Chemical used

The chemical used and their sources are given in following table. All chemical were used as these were obtained in the laboratory.

**Table 2.1:** Chemicals used along with their source

| Chemicals | Short name | Source |
|---|---|---|
| Copper sulphate | $CuSo_4.5H_2O$ | CDH |
| Ammonium solution | $NH_3$ | THOMAS BAKER |
| Sodium dodecyle benzene sulphonate | SDBSA | HIMEDIA |
| Aniline | ANI | SRL |
| Hydrochloric acid | HCl | SRL |
| Ammonium persulfate | APS | MERCK |
| Hydrogen peroxide | $H_2O_2$ | THOMAS BAKER |
| Monobasic sodium phosphate | $NaH_2PO_4$ | CDH |
| Di-basic sodium phosphate | $Na_2HPO_4$ | CDH |

## 2.2 Apparatus

X-ray diffraction (XRD) studies have been carried out to characterize the structure and particle size of CuO nanostructure and CuO/PANI nanocomposite using Bruker D8 Advance Diffractometer with Ni-filtered Cu Kα radiation (IIT, New Delhi) with Voltage- 30 kV, 35 mA. The surface morphological studies of $CuO_2$, PANI and CuO/PANI film have been investigated using scanning electron microscope (HITACHI, Model No.S-3700N with EDS-X with X-ray). The atomic force microscopic studies have been done using Park Systems, XE-100. Transmission electron microscopy was done for the CuO nanostructure using FEI Tecnai S Twin (AIIMS, New Delhi). Fourier transform infrared (FTIR) spectrophotometer (Thermoscientific, Nicolet-380) has been used to characterize CuO/PANI nanocomposite. The UV-visible spectroscopic studies have been conducted on UV/VIS/NIR spectrometer (Perkin Elmer, Lambda 950). The PL emission studies have been done using Fluorolog 3, made by Horiba. The electrochemical studies and amperometric measurements have been recorded on an Auto lab Potentiostat/Galvanostat (Metrohm). The electrochemical measurements have been conducted on a three-electrode system with CuO/PANI/ITO electrode as the working electrode, a platinum (Pt) wire as the counter electrode, and saturated Ag/AgCl electrode as a reference electrode in phosphate buffer saline (5 mM, pH 7.5, 0.9% NaCl) containing 5 mM $[Fe(CN)_6]^{3-/4-}$ mediator.

## 2.3 Methods

### *2.3.1 Preparation of CuO nanostructure by sol-gel method*

**Sol-gel method:** Sol-gel method is a versatile process used in making various oxide nanomaterials. In the sol-gel method, a colloidal suspension, or a sol is formed from hydrolysis and polymerization reactions of the precursors, which are usually metal salts or metal organic compounds such as metal alkoxide. Complete polymerization and loss of solvent leads to transition from the liquid sol into a solid gel phase. Thin films of sol can be produced on a piece of substrate by spin-coating and dip-coating. A wet gel forms when the sol is cast into a mold, which gets converted dense ceramic with further drying and heat treatment. Sol-gel derived nanomaterials films have acquired much attention owing to various advantages such as low-temperature process ability, large surface area, tunability, thermal stability, biocompatibility and cost-effectiveness

***Synthesis***

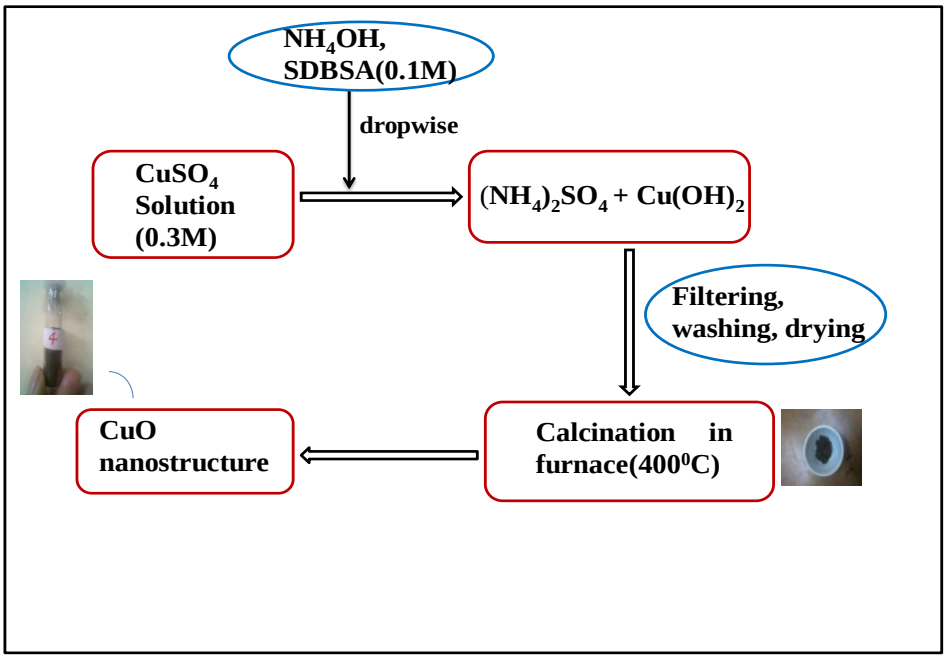


**Fig. 2.1:** Schematic picture of synthesis of CuO nanostructure

Dissolve 0.3 M $CuSO_4.5H_2O$ in 100 ml distilled water at magnetic stirrer for ½ h. After several minutes solution shows like light blue colour. Drop wise $NH_3$ solution added into the above solution till pH12 is reached. Dark blue colour is obtained. That solution stirring for 6 h. 0.1M SDBSA solution prepared in 20 ml distilled water. 2 ml solution of SDBSA added into the copper sulphate solution and rotated for 2 h. After that above solution kept in water bath at 50-60$^0$C for 2 h till bubbles settles and quenched in cold water. Filtered the solution. Washed several times till pH 7 is reached. Dried in oven at 50-60$^0$C. Dried sample put on crucible and calcinations at 400$^0$C for 6 h. Sample crushed and filled in glass vial.

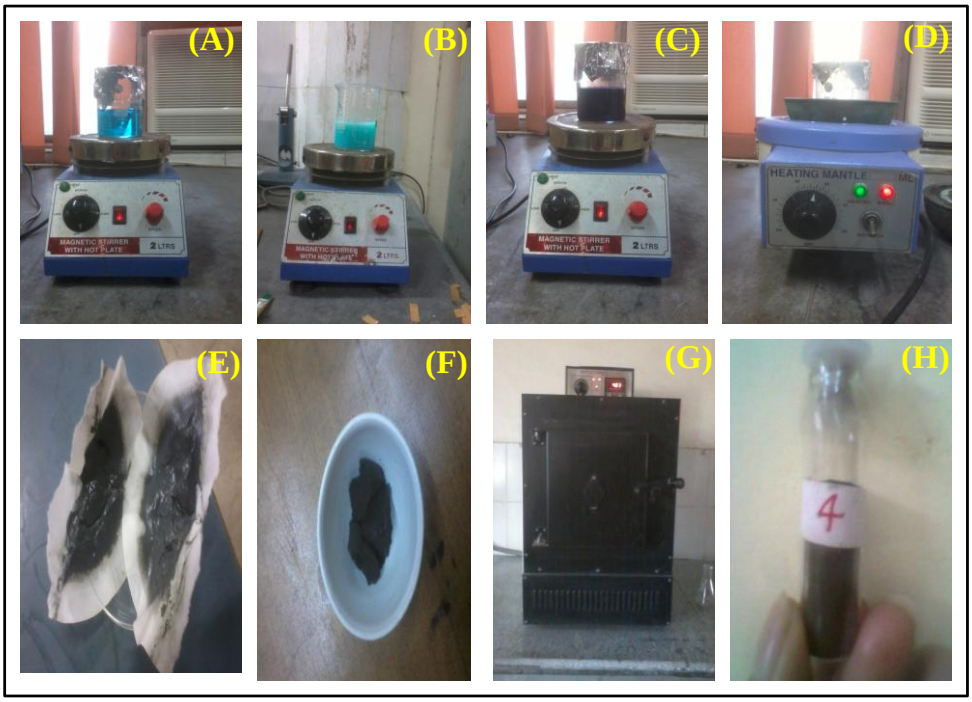


**Fig. 2.2: A-H** showing the experimental synthesis process of CuO nanostructure

### *2.3.2 Preparation of PANI by ultrasonic method*

In ultrasonic synthesis method, 4 mmol aniline was dissolved in 20 ml hydrochloric acid (1M) and stirred with magnetic stirrer for one hour. 4mmol ammonium persulfate was also dissolved in 20 ml hydrochloric acid (1 M) and magnetically stirred for one hour. Then, the aniline solution was kept in the ultrasonic machine for 20 min. The ammonium persulfate solution was added into the aniline solution drop by drop and was kept at the ultrasonicator till the ammonium per sulphate solution is completely added. After that for one more hour the solution is ultrasonicated as the black green precipitate was being formed inside the beaker. After that it was kept at room temperature overnight. Finally, the black green precipitate was collected and washed several times by acetone and distilled water. The pure polyaniline was then dried at ambient temperature for 24 h.

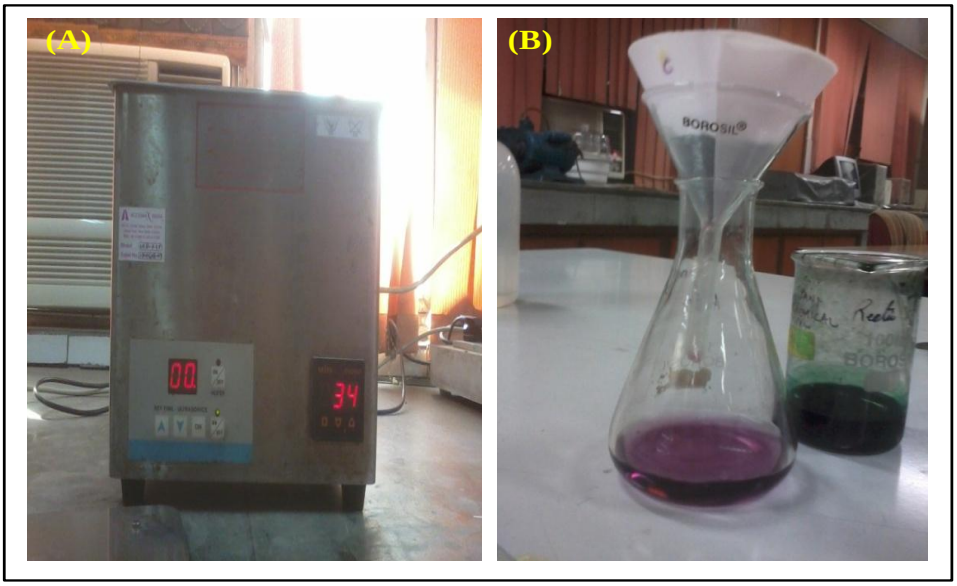


**Fig.2.3:** (A) Ultrasonicator instrument (B) filtering process during PANI synthesis

### *2.3.3 Functionalization of ITO (Indium Tin Oxide) glass plates*

ITO (Indium Tin Oxide) coated glass sheets were cut into small pieces (0.5cm×2cm) and immersed in a solution of $H_2O_2$:$NH_3$:$H_2O$ in the ratio of 1:1:5 (v/v) respectively and then kept under oven for 1h at 80$^oC$ to obtain uniformly distributed OH groups on the ITO surface. Further the functionalized ITO plates were washed with de-ionized water and dried at room temperature. After that ITO plates were cleaned with acetone and stored in dust free environment for future use.

### *2.3.4 Preparation of CuO/PANI/ITO electrode*

Electrophoretic deposition (EPD) was carried out by using DC battery (Bio-Rad, model 200/2.0). The 25 mg CuO nanostructure and 25 mg PANI were dispersed in 5 ml of double DI water followed by ultrasonication (30 min). A platinum foil (1cm×2cm) was used as the cathode and a hydrolyzed ITO-coated glass plate was used as anode. The ITO electrode was washed with diluted ammonia, ethanol and water respectively. The two electrodes, placed parallel to each other with separation of 1cm, were dipped in the colloidal suspension of CuO and PANI. The film deposition was carried out ITO plate (0.25 $cm^2$) at 30 mV for 50 s. the

film were then removed from the suspension followed by washing with DI water to remove any unbound particles.

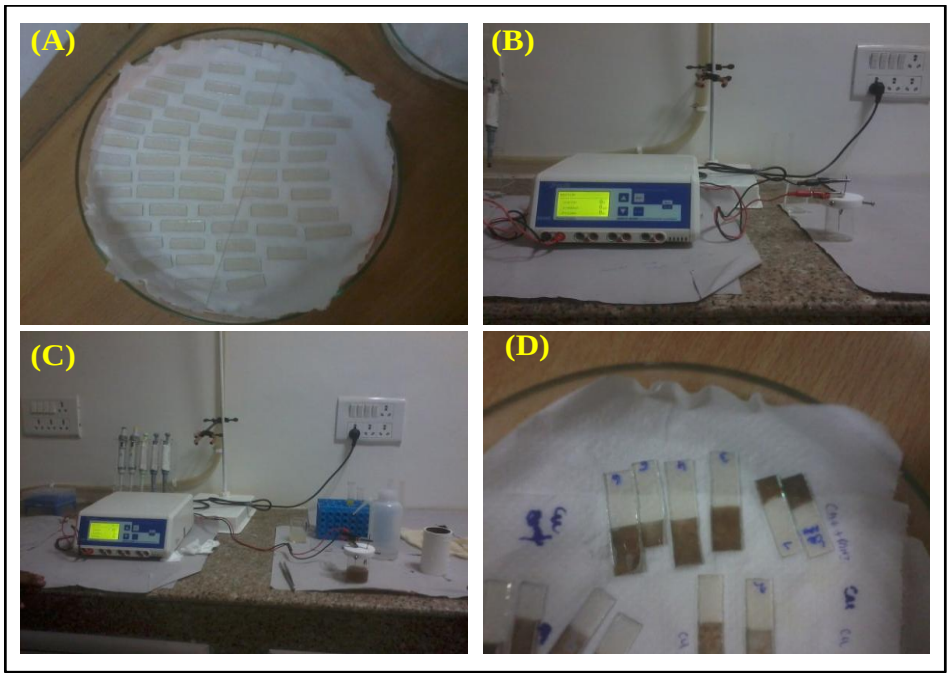


**Fig.2.4:** showing process for Preparation of CuO/PANI/ITO electrode

### *2.3.5 Preparation of phosphate buffer solution*

Phosphate buffer solution was prepared by mixing of two freshly prepared solutions, solution-A and solution-B. Solution-A was prepared by dissolving 6 gm of monobasic sodium phosphate (sodium di-hydrogen phosphate, $NaH_2PO_4$) in 250 ml of de-ionized water and Solution-B was prepared by dissolving 7.1 gm of dibasic sodium phosphate (disodium hydrogen phosphate, $Na_2HPO_4$) in 250 ml of de-ionized water. Now the phosphate buffer solution of different pH can be obtained by mixing different proportion of solution-A and solution-B (X ml of Solution-A + Y ml of solution-B, diluted to a total of 200 ml).

Now the phosphate buffer solution of different pH can be obtained by mixing different proportion of solution-**A** and solution-**B** (X ml of Solution-**A** + Y ml of solution-**B**, diluted to a total of 200 ml).

For pH 5.7: (93.5 ml of solution-**A** + 6.5 ml of solution-**B**) + 100 ml of DI water.
For pH 6.0: (87.7 ml of solution-**A** + 12.3 ml of solution-**B**) + 100 ml of DI water.
For pH 7.0: (39 ml of solution-A + 61 ml of solution-B) + 100 ml of DI water.
**For pH 7.5: (16 ml of solution-A + 84 ml of solution-B) + 100 ml of DI water.**
For pH 8.0: (5.3 ml of solution-**A** + 94.7 ml of solution-**B**) + 100 ml of DI water.

### *2.3.6 Preparation of phosphate buffer saline solution*

Phosphate buffer saline (PBS) solution was prepared by the addition of 0.9% of NaCl salt per 200 ml of phosphate buffer solution. Now 0.422 gm of potassium ferrocyanide $\{K_4Fe(CN)_6\}$ and 0.329 gm of potassium ferricyanide $\{K_3Fe(CN)_6\}$ were added to the PBS as mediator and shake well until it became yellowish clear solution. PBS solution was usually stored under refrigerated condition ($4^{\circ}C$) when not in use.

### *2.3.7 Preparation of hydrogen peroxide ($H_2O_2$) solution of different molarity*

The solution of $H_2O_2$ ($M_w$ = 50.06) taken was 20.58 M. Solutions of different working concentration of $H_2O_2$ (like 2, 5, 8, 12, 15, 20, and 22 mM) solutions were prepared by serial dilution with de-ionized water.

### *2.3.8 Antibacterial performance*

**Table 2.2:** Preparation of Nutrient Agar Media

| **Ingredients** | **g/ l** |
|---|---|
| Peptone | 5.000 |
| Beef Extract | 3.000 |
| Agar | 15.000 |

***Preparation***

Suspended 28 gm in 1000 ml distilled water. Heated to boiling to dissolve the medium completely. Sterilized by autoclave at 15 psi pressure (121°C) for 15 min. The contents were mixed well before dispensing.

The antibacterial activity of the synthesized CuO nanostructures, PANI, and the CuO/PANI nanocomposite was evaluated by swabbing method against *B. cereus* and *P. aeruginosa*. First of all, nutrient agar media was prepared in the autoclave at 121°C at 15 psi. After release of pressure from the autoclave, the media was poured aseptically into the petri plates in laminar air flow. The plates were allowed to cool down inside the laminar air flow so as to solidify the agar. After that bacterial colonies were picked from the sub cultured bacterial plates with the help of autoclaved cotton swabs. The cotton swab was dipped into autoclaved normal saline solution (0.9% NaCl solution) and then used to pick the bacterial colony. The swab was rubbed into the respective agar plate thoroughly at 360°. The agar plates were kept still for 10 min so that the bacterial culture gets little absorbed into the media. Then the wells were created in the swabbed agar plate for 4 samples using autoclaved wire loop. 30-40 µl samples were added into the respective wells in desired concentrations. CuO nanostructure, PANI, CuO/PANI nanocomposite and water as a control were taken in 1 mg/ml concentration. The same steps were performed for testing antibacterial activity against both *B. cereus* and *P. aeruginosa*. Now, both the bacterial plates with loaded wells were incubated at 37 °C +/- 2 °C for 24 h in BOD incubator. Next day the respective value of the inhibition zones were collected.

## 2.4 Characterisation Techniques

### 2.4.1 Morphological characterisation

#### *2.4.1.1 Scanning electron microscopy (SEM)*

A scanning electron microscope (SEM) is a type of electron microscope that develops images of a sample by scanning it with a sharpened beam of electrons. The electrons interact with atoms in the sample, producing various signals that can be detected and that contain information about the sample's surface topography and composition. The electron beam is generally scanned in a raster scan pattern, and the beam's position is combined with the detected signal to produce an image.

The SEM used was from HITACHI, Model No.S-3700N with EDS-X with X-ray.

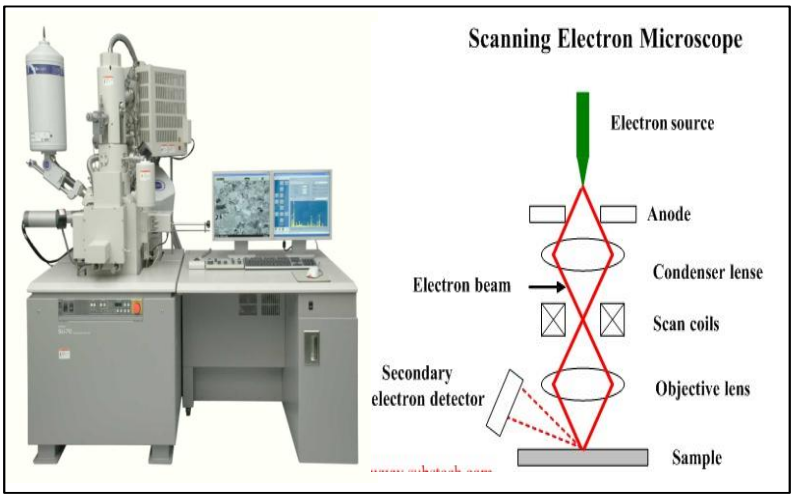


**Fig. 2.5:** Scanning electron microscope

#### *2.4.1.2 Atomic force microscopy (AFM)*

Atomic force microscopy is a very high resolution type of scanning probe microscopy, with demonstrated resolution on the order of fraction of a nanometer, more than 1000 times better than the optical. It provides a 3D profile of the surface on a nanoscale, by measuring forces between a sharp probe (<10 nm) and surface at very short distance (0.2 to 10 nm probe-

sample separation). The probe is supported on a flexible cantilever. The AFM tip gently touches the surface and records the small force between the probe and the surface. It measures the forces acting between a fine tip and a sample. The tip is attached to the free end of a cantilever and is brought very close to a surface. Attractive or repulsive forces resulting from interactions between the tip and the surface will cause a positive or negative bending of the cantilever. There are 4 ways of using AFM:-

- Imaging- determing the topography of the surface.
- Measuring-characterizing the sample's materials properties.
- Manipulating- purposefully changing the surface structure.
- Sensing- using AFM technology for sensor applications.

The measurement of an AFM is made in three dimensions. The horizontal x-y plane and vertical z dimension. Resolution (magnification) at z-direction is normally higher than x-y.

Mode of operation:

- Contact AFM: < 0.5 nm probe-surface separation
- Tapping mode AFM: 0.5- to 2 nm probe-surface separation
- Non-contact AFM: 0.1 to 10 nm probe-surface separation

In contact-mode the tip either scans at a constant small height above the surface or under the conditions of a constant force. In the constant height mode the height of the tip is fixed, whereas in the constant-force mode the deflection of the cantilever is fixed and the motion of the scanner in z-direction is recorded. Silicon nitrides are used for contact mode.

In non-contact mode probe does not contact the sample surface, but oscillates tips on the surface during scanning. The tip is oscillated at the resonance frequency and the amplitude of the oscillation is kept constant. The probe operates in the attractive force region and tip sample interaction is minimized. The use of non-contact mode allowed scanning without influencing the shape of the sample by the tip-sample forces. The tips mainly used for this mode are silicon probe.

In tapping mode force that act between the sample and the tip will not only cause a change in the oscillation amplitude, but also change in the resonant frequency and phase of the cantilever.


**Fig. 2.6:** Atomic force microscope

### 2.4.1.3 Transmission electron microscopy (TEM)

TEM is a microscopy technique in which a beam of electrons is transmitted through an ultra-thin specimen, interacting with the specimen as it passes through. An image is formed from the interaction of the electrons transmitted through the specimen. The image is magnified and focused onto an imaging device, such as a fluorescent screen, on a layer of photographic film, or to be detected by a sensor such as a CCD camera.

TEM are capable of imaging at a significantly higher resolution than light microscopes, owing to the small de Broglie wavelength of electrons. This enables the instrument's user to examine fine detail-even as small as a single column of atoms, which is thousands of times smaller than the smallest resolvable object in a light microscope. TEM forms a major analysis method in a range of scientific fields, in both physical and biological sciences. TEMs find application in cancer research, virology, materials science as well as pollution, nanotechnology and semiconductor research.

At smaller magnifications TEM image contrast is due to absorption of electrons in the material, due to the thickness and composition of the material. At higher magnifications complex wave interactions modulate the intensity of the image, requiring expert analysis of observed images. Alternate modes of use allow for the TEM to observe modulations in

chemical identity, crystal orientation, electronic structure and sample induced electron phase shift as well as the regular absorption based imaging.

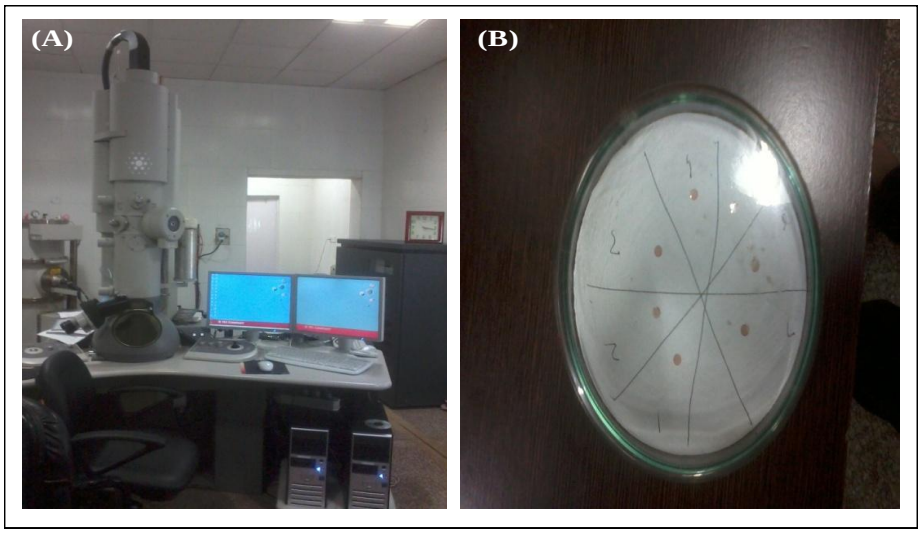


**Fig. 2.7:** (A) Transmission electron microscope (B) TEM grid

### 2.4.2 Structural characterisation

#### *2.4.2.1 Photoluminescence (PL)*

PL is light emission from any form of matter after the absorption of photons (electromagnetic radiation). It is one of many forms of luminescence (light emission) and is initiated by photoexcitation (excitation by photons). The excitation typically undergoes various relaxation processes and then photons are re-radiated. The period between absorption and emission can be extremely short. It range is femtosecond for the emission.eg-free carrier plasma in inorganic semiconductors up to milliseconds for phosphorescent processes in molecular systems. However, it can be extended into minutes or hours under special circumstances.

The observation of photoluminescence at certain energy can be seen most straightforwardly as indication of population of the state associated with this transition energy. While this is generally true in atoms and similar systems, correlations and other more complex phenomena

also act as sources for photoluminescence in many body systems such as semiconductors. A theoretical approach to handle this is given by the semiconductor luminescence equations.

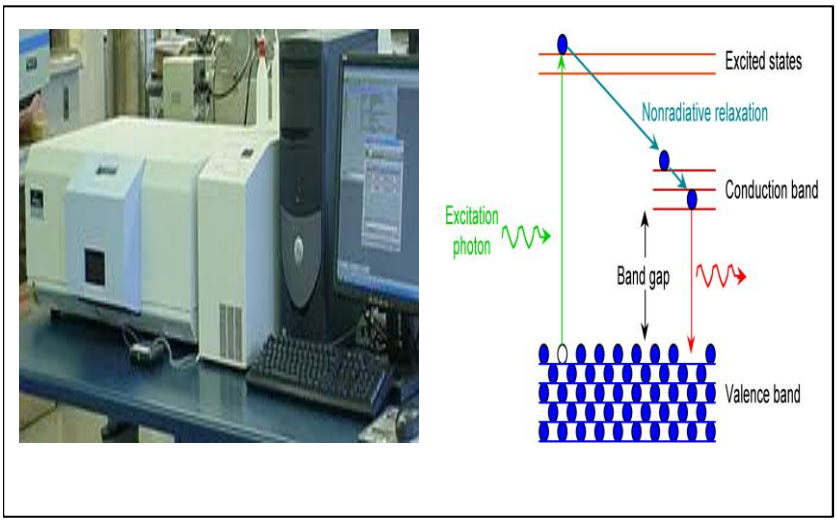


**Fig. 2.8:** photoluminescence spectrophotometer

### *2.4.2.2 UV-Visible Spectroscopy*

Ultraviolet-visible spectrophotometer (UV-Vis or UV/Vis) refers to absorption spectroscopy or reflectance spectroscopy in the ultraviolet-visible spectral region. This means it uses light in the visible and adjacent (near UV and near infrared ranges. The absorption or reflectance in the visible range directly affects the perceived colour of chemicals involved. In this region of the electromagnetic spectrum, molecules undergo electronic transitions. This technique is complementary to florescence spectroscopy, in that florescence deals with transitions from the excited state to the ground state, while absorption measures transitions from the ground state to the excited state. Molecules containing π-electrons or non-bonding electrons (n-electrons) can absorb the energy in the form of ultraviolet or visible light to excite these electrons to higher anti-bonding molecular orbitals. The more easily excited the electrons (i.e. lower energy gap between the HOMO and the LUMO), the longer the wavelength of light it can absorb.

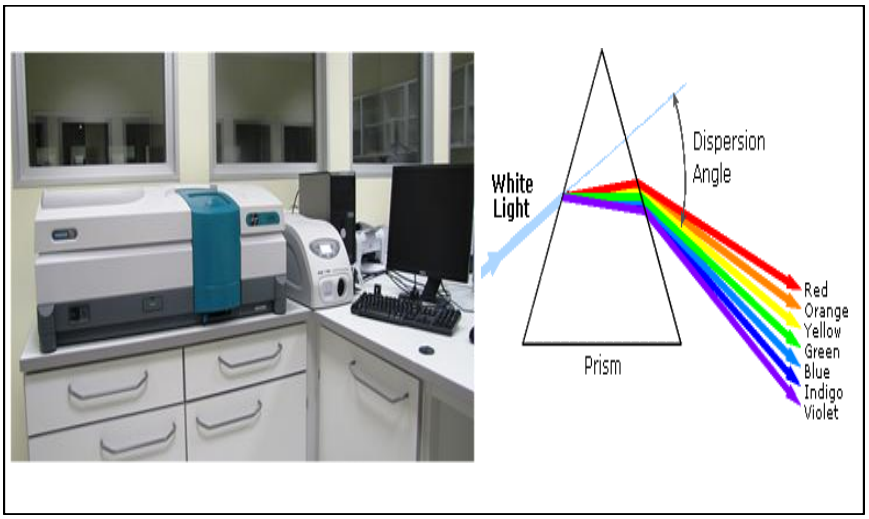


**Fig. 2.9:** UV-Visible Spectrophotometer

### *2.4.2.3 Fourier Transform Infrared Spectroscopy (FTIR)*

FTIR stands for Fourier Transform Infrared, the preferred method of infrared spectroscopy. In infrared spectroscopy, IR radiation is passed through a sample. Some of the infrared radiation is absorbed by the sample and of it is passed through (transmitted). The resulting spectrum represents the molecular absorption and transmission, creating a molecular fingerprint of the sample. Like a fingerprint no two unique molecular structures produces the same infrared spectrum. This makes infrared spectroscopy useful for several types of analysis.

FTIR can provide following information:

- It can identify unknown materials
- It can determine the quality or consistency of a sample
- It can determine the amount of components in a mixture

An infrared spectrum represents a fingerprint of a sample with absorption peaks which correspond to the frequencies of vibrations between the bonds of the atoms making up the materials. Because each different material is a unique combination of atoms, no two compounds produce the exact same infrared spectrum. Therefore, infrared spectroscopy can result in a positive identification (qualitative analysis) of every different kind of material. In

addition, the size of the peaks in the spectrum is a direct indication of the amount of material present. With modern software algorithms, infrared is an excellent tool for quantitative analysis. The FTIR used in this project is Thermoscientific, Nicolet-380.

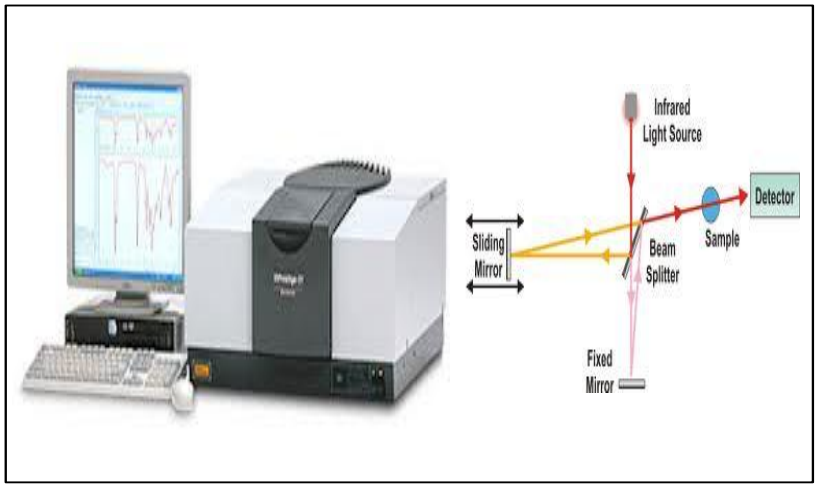


**Fig. 2.10:** Fourier Transform Infrared Spectroscope`

### *2.4.2.4 X-ray Diffraction (XRD)*

X-ray powder diffraction (XRD) is a rapid analytical technique primarily used for phase identification of crystalline material and provides information on unit cell dimensions. The analyzed material is finely ground, homogenized, and average bulk composition is determined. Crystalline substances act as three-dimensional diffraction gratings for x-ray wavelength similar to the spacing of planes in a crystal lattice. X-ray diffraction is now a common technique for the study of crystal structures and atomic spacing.

X-ray diffraction is based on constructive interference of monochromatic X-rays and a crystalline sample. These X-rays are generated by a cathode ray tube, filtered to produce monochromatic radiation, collimated to concentrate, and directed toward the sample. The interaction of the incident rays with the sample produces constructive interference (and a diffraction ray) when conditions satisfy Bragg's Law ($n\lambda=2d\ \sin\Theta$). This law relates the wavelength of electromagnetic radiation to the diffraction angle and the lattice spacing in a

crystalline sample. These diffracted X-rays are then detected, processed and counted. By scanning the sample through a range of 2Θ angles, all possible diffraction directions of the lattice should be attained due to the random orientation of the powdered material. Conversion of the diffraction peaks to d-spacing allows identification of the mineral because each mineral has a set of unique d-spacing. Typically, this is achieved by comparison of d-spacing with standard reference patterns.

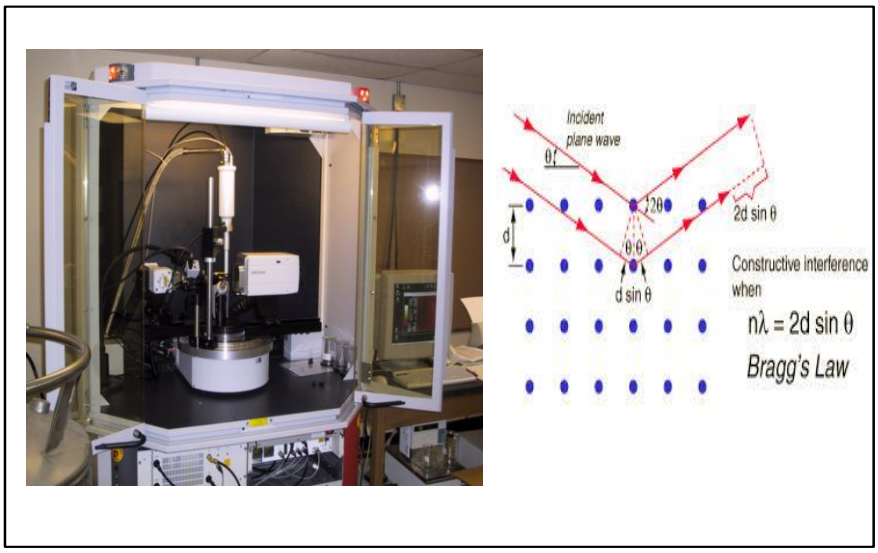


**Fig. 2.11:** X-ray Diffraction pattern

All diffraction methods are based on generation of X-rays in an X-ray tube. These X-rays are directed at the sample, and the diffracted rays are collected. A key component of all diffraction is the angle between the incident and diffracted rays.

### 2.4.3 Electrochemical Techniques

Electrochemistry is a branch of chemistry that studies chemical reactions which take place in a solution at the interface of an electron conductor (the electrode: a metal or a semiconductor) and an ionic conductor (the electrolyte). These reactions involve electron transfer between the electrode and the electrolyte or solution. Thus electrochemistry deals with interactions between electrical energy and chemical change and vice versa.

If a chemical reaction is driven by an externally applied voltage, as in electrolysis, or if a voltage is created by a chemical reaction as in a battery. It is an electrochemical reaction. In contrast, chemical reactions where electrons are transferred between molecules are called oxidation-reduction (redox) reactions. In general, electrochemistry deals with situations where redox reactions are separated in space or time, connected by an external electric circuit.

Electrochemical processes involving electron transfer to or from a molecule or ion changing its oxidation state. Oxidation and reduction describe the change of oxidation state that takes place in the atoms, ions or molecules involved in an electrochemical reaction. The atom or molecule which loses electrons is known as the reducing agent, or reductant, and the substance which accepts the electrons is called the oxidizing agent, or oxidant. Thus, the oxidizing agent is always being reduced in a reaction; the reducing agent is always being oxidized.


**Fig. 2.12:** Auto lab/potentiostat instrument set up

In a solution, the equilibrium concentrations of the reduced and oxidized forms of a redox couple are linked to the potential E via the Nernst's Equation.

$$E = E_0 + \frac{RT}{nF} \ln \frac{C_{oxi}}{C_{red}}$$

Where, $E_0$ is equilibrium potential, F is Faradays constant, T is absolute temperature, $C_{oxi}$ and $C_{red}$ are concentrations of oxidation and reduction centres. For each redox couple, there exists a potential, known as the standard potential $E_0$ at which the reduced and oxidized forms are present at equal concentrations. If the potential E with respect to the reference electrode is applied to the working electrode, e.g. by the use of a potentiostat, the redox couples present at the electrode respond to this change and adjust their concentration ratios according to above Eq. The analysis of the measured parameters namely current or voltage helps in identification and quantification of the species under studies. This method facilitates performing various electrochemical experiments in a single unit. There are various electrochemical methods listed below.

- **Normal pulse voltammeter**
- Constant current (chronopotentiommetry)
- Constant voltage (chronoamperommetry)
- Normal pulse stripping voltammetry
- **Differential pulse voltammetry**
- Differential pulse stripping voltammetry
- Square wave voltammetry
- Square wave stripping voltammetry
- Colourmetry
- Potentiometric stripping analysis (PSA)
- pH/milivolts measurement

### *2.4.3.1 Cyclic voltammetry (CV)*

Cyclic voltammetry is a type of potentiodynamic electrochemical measurement. To obtain a cyclic voltammogram, the voltage is varied in a solution and change in current is measured with respect to the change in voltage. It is a useful and versatile electroanalytical technique for studying the redox properties of electroactive species. In a CV experiment, the current increases as the potential reaches the oxidation potential of the analyte, where after it falls off as the concentration of the analyte is depleted close to the electrode surface. At this potential (often referred to as a switching potential), the direction of the potential scan is reversed, and the same potential window is scanned in the opposite direction (hence the term cyclic). As the applied potential is reversed, it will reach a potential where the reduction of product formed during forward scan starts producing a current of reverse polarity from the forward scan. This reduction peak will usually have a similar shape as that of an oxidation peak in other direction.

### *2.4.3.2 Differential Pulse Voltammetry (DPV)*

This technique is comparable to normal pulse voltammetry in that the potential is scanned with a series of pulses. However, it differs from NPV because each potential pulse is fixed, of small amplitude (10 to 100 mV), and is superimposed on a slowly changing base potential. Current is measured at two points for each pulse, the first point (1) just before the application of the pulse and the second (2) at the end of the pulse. These sampling points are selected to allow for the decay of the non-faradic (charging) current. The difference between current measurements at these points for each pulse is determined and plotted against the base potential.

### 2.3.4 Antibacterial activity

The ledge life of a product can be stretched either by contributing artificial preservatives or by accepting hygienic measures throughout the constructing process. As the consumer style today is towards preservative-free foods with a long ledge life, industry is being pushed to reconsideration its constructing methods. Instead of contributing preservative agents, enhanced hygienic safeguards can be accepted during production. A hygienic and clean manufacturing environment is required in order to maintain contamination-referred reject rates low. The usage of surfaces in the constructing environment with antibacterial props can significantly reduce contamination risks.

The conclusion of the antibacterial activity of surfaces is reported in the following norms: ISO 22196 and JIS Z 2801. The Japanese norm JIS Z 2801 was issued in 2000 and issued again in 2007 as the internationally sensible norm ISO 22196. So, ISO 22196 and JIS 2801 are identical. In the test, surface system without an antibacterial coating and surface system coated with sporicide are charged with selected microorganisms.

The reduction factor is followed out after 24 hours by finding out colony counts on the reference surface and on the antibacterial surface.

# 3 RESULTS ANS DISCUSSION

## 3.1 Morphological studies

### *3.1.1 Scanning electron microscope (SEM) and Element detection X-ray spectrum (EDS) studies*

***SEM:*** The SEM images of the PANI, CuO nanostructure and CuO/PANI nanocomposite are depicted in figure 3.1, 3.2 and 3.3 respectively. The partial crystalline nature of PANI illustrates nanofibre like morphology. Different parameters are responsible to control the morphology of PANI such as type of acidic dopants and oxidants. Another important factor which might influence on the morphology of the PANI nanofibre is the aniline/oxidant molar ratio. CuO found to be nanorod-like structure. CuO/PANI/ITO electrode has agglomerated structure. During the formation of nanocomposite, nanofibre of PANI and nanorod of CuO are mixed.

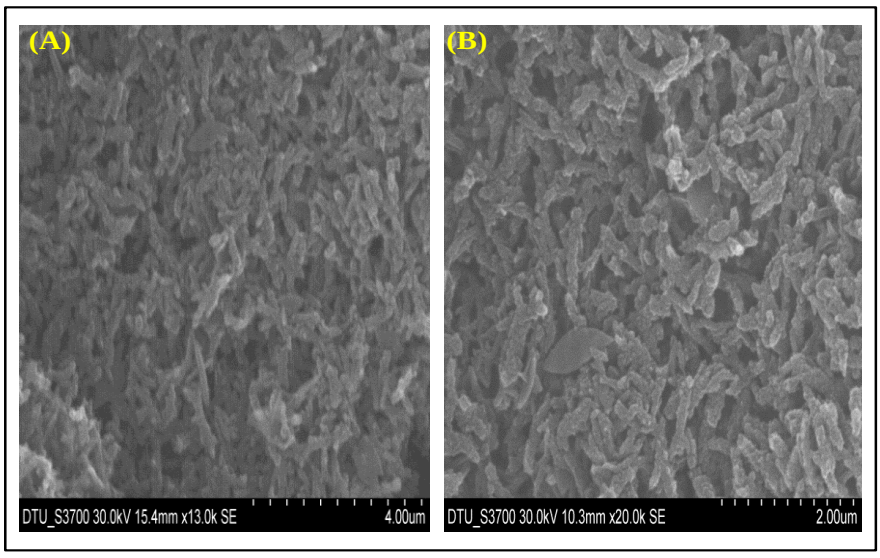


**Fig. 3.1:** SEM images of PANI nanofibre

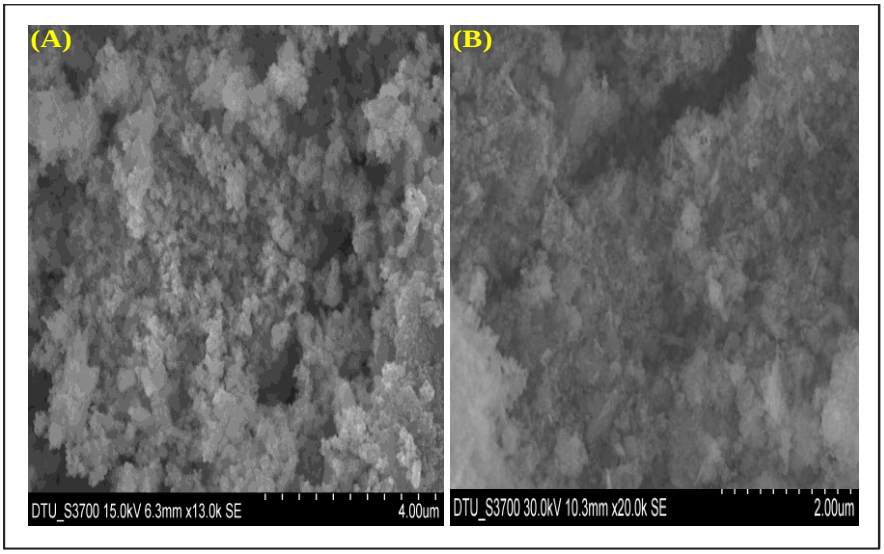


**Fig. 3.2:** SEM images of nanostructured CuO

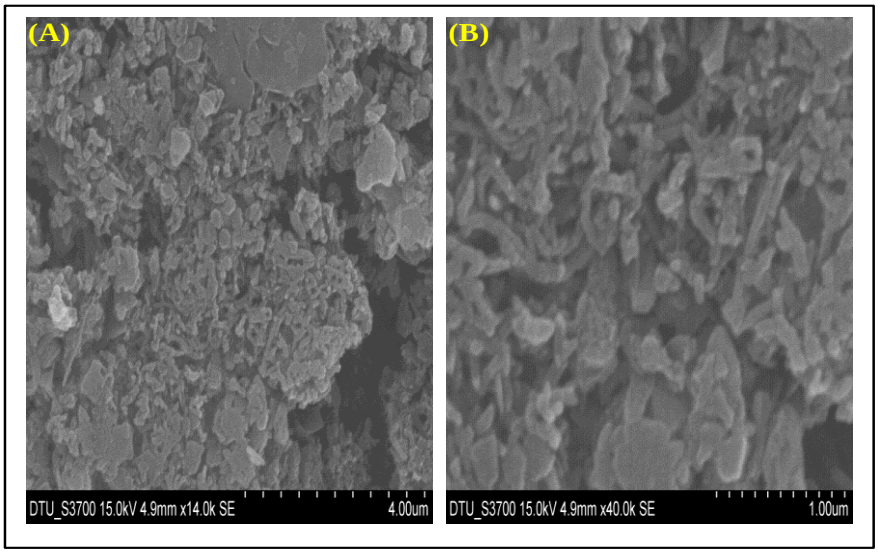


**Fig. 3.3:** SEM images of CuO/PANI nanocomposites film

***EDS:*** The EDS graphs of the PANI, nanostructured CuO and CuO/PANI/ITO electrode are showing in figure 3.4, 3.5 and 3.6. According to EDS spectrum carbon and nitrogen element are detected in the prepared PANI sample. Weight % of carbon and nitrogen are not showing in table because these are traces element but atom% is observed C 29.32% and N 70.68%.

Figure 3.5 depicts the EDS spectrum exposes that only Cu and O element are observed in the synthesized CuO powder. There are not found any traces of other impurities like carbon etc.

the weight % of copper and oxide detected from EDS is O 22.98wt% and Cu 77.02wt%. The weight Cu/O ratio can be calculated to be 3.35, which is close to actual value of 4 for CuO. So the result of EDS analysis confirmed that the produced powder is CuO.

From the EDS analysis we obtained the constituent element present in prepared sample. In case of CuO/PANI nanocomposite we found C, N, Cu and O elements from EDS detection. Figure 3.6 shows atomic % of C=32.27%, N= 19.73%, O= 21.43% and Cu= 26.57% there are some trace elements are present like carbon and nitrogen. Presence of carbon and nitrogen we say those CuO/PANI nanocomposite are formed because polyaniline structure have C and N element. So the result of EDS analysis confirmed that produced ITO film has nanocomposite characteristics.

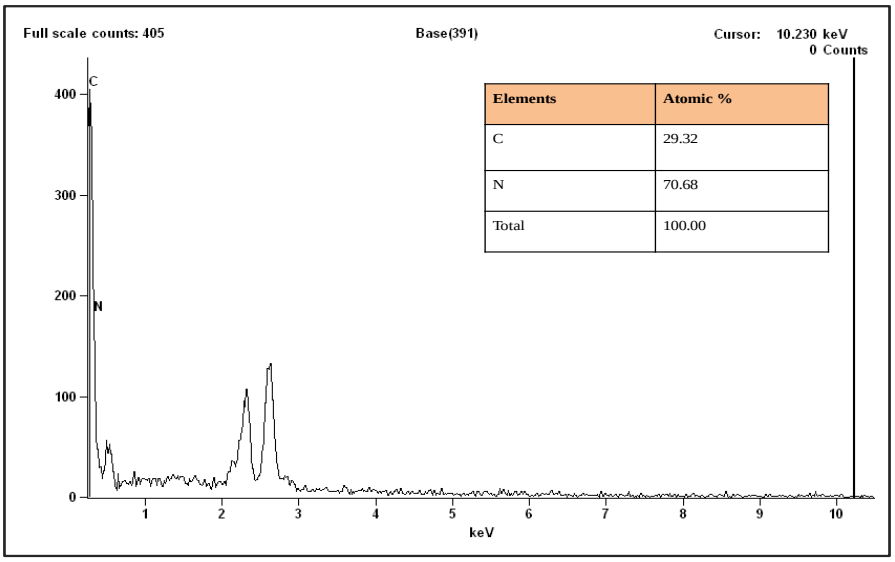


**Fig. 3.4:** EDS spectra of PANI

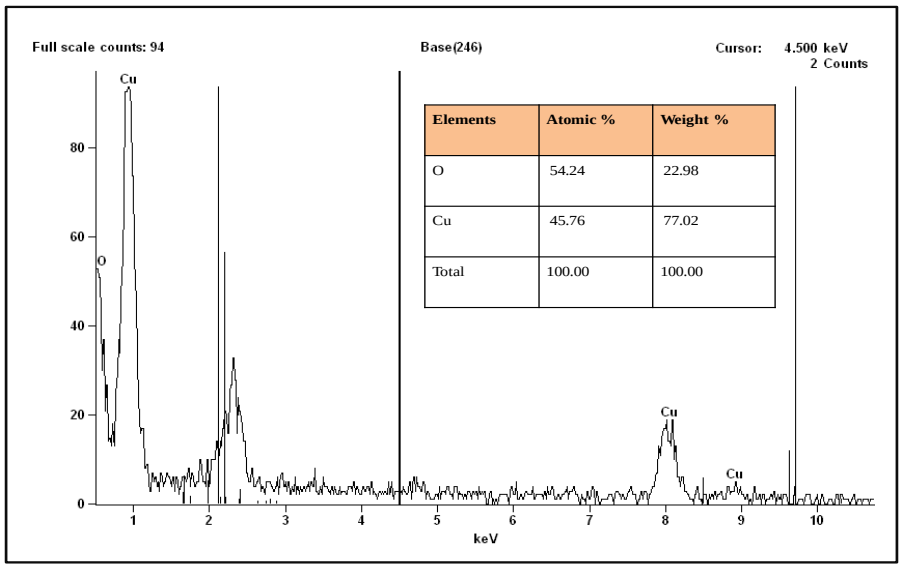


| Elements | Atomic % | Weight % |
|---|---|---|
| O | 54.24 | 22.98 |
| Cu | 45.76 | 77.02 |
| Total | 100.00 | 100.00 |

**Fig. 3.5:** EDS spectra of nanostructured CuO

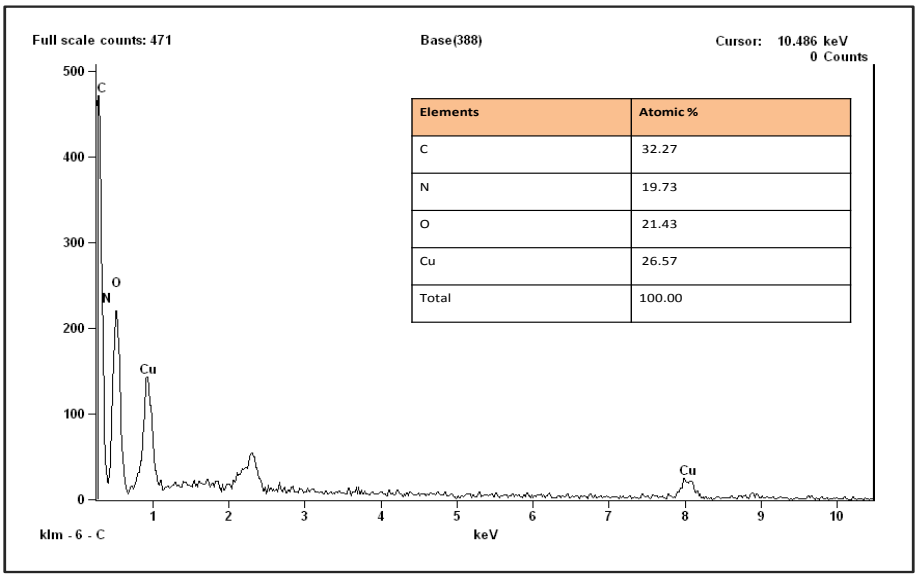


| Elements | Atomic % |
|---|---|
| C | 32.27 |
| N | 19.73 |
| O | 21.43 |
| Cu | 26.57 |
| Total | 100.00 |

**Fig. 3.6:** EDS spectra of CuO/PANI nanocomposites

### *3.1.2 Atomic force microscopy (AFM)*

AFM studies were accomplished to enquire the surface properties for PANI/ITO film, CuO/ITO nanostructure film and CuO/PANI/ITO nanocomposite film electrode in air environment. Figure shows 2D and 3D AFM images of PANI, CuO nanostructures and CuO/PANI/ITO electrode. Uniform height distribution surface is seen in 3D view.

Figure 3.7 shows the surface morphology of PANI/ITO film. Smooth, bulbous and homogeneous particles found in structure.

Figure 3.8 shows the 2D and 3D structure of CuO nanostructure that exhibit uniformly distributed copper oxide. Root mean square roughness's (Rq)-8.459 nm, average roughness (Ra)-6.209 nm and maximum profile peak height-74.186 nm were found.

Figure 3.9 established the 2D and 3D morphology of CuO/PANI/ITO nanocomposite film which shows that CuO nanostructure mixed with PANI with root mean square roughness (Rq)-4.948 average roughnesses (Ra)-3.566 nm, maximum profile peak height-24.975 nm. It can be seen that roughness is decreased as compare to the CuO/ITO nanostructure surface because of PANI. So we obtained smoothed nanocomposite film.

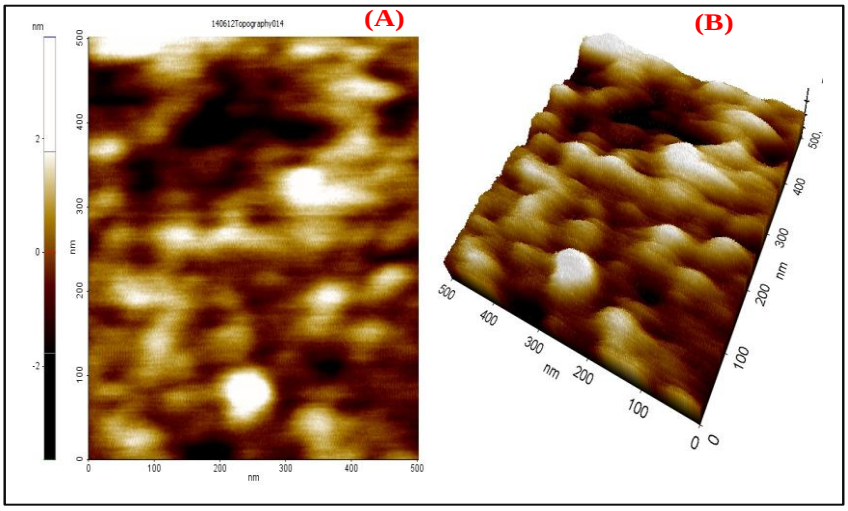


.**Fig. 3.7:** AFM images of PANI (A) front view(2D) (B) 3-D view

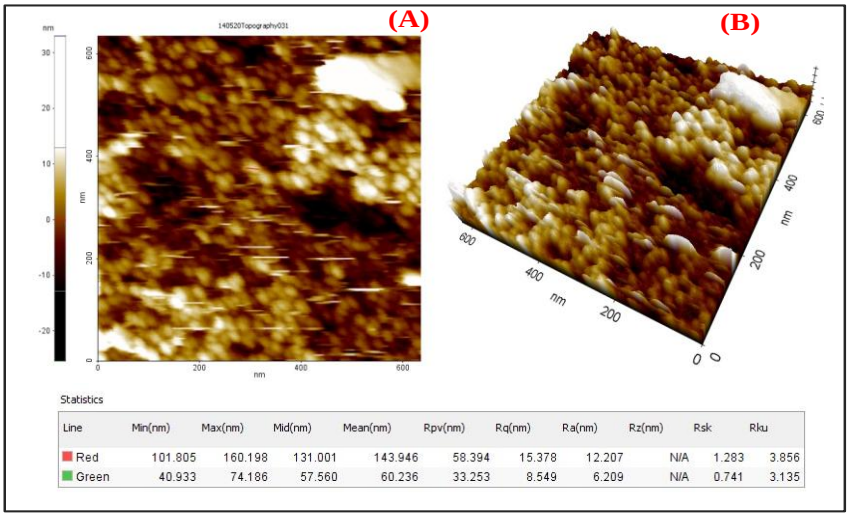


**Fig. 3.8:** AFM images of nanostructured CuO (A) front view(2D) (B) 3-D view

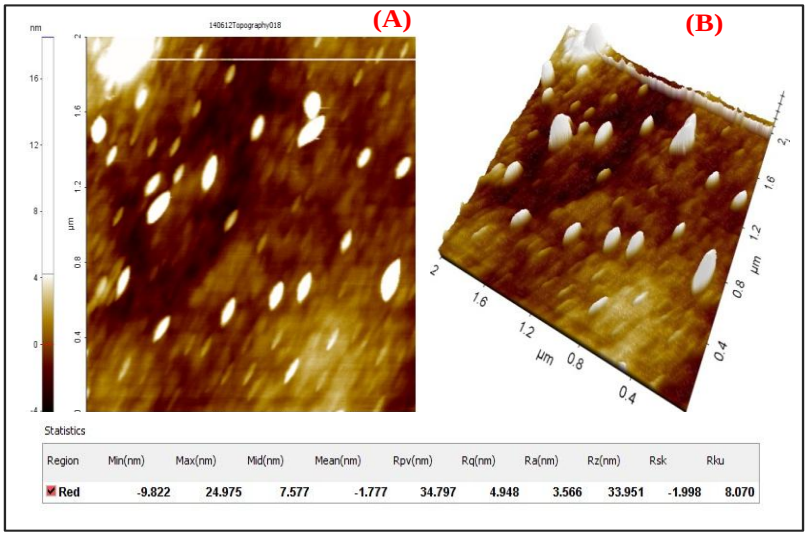


**Fig. 3.9:** AFM images of CuO/PANI/ITO electrode (A) front view(2D) (B) 3-D view

### *3.1.3 Transmission electron microscopy (TEM)*

Figure 3.10 indicates TEM micrograph of the synthesized CuO nanostructures. Images shows agglomerations of nanoscale are clearly observed. The TEM graph is also showed that the CuO nanostructures are rod type in shape and agglomerated to each other.

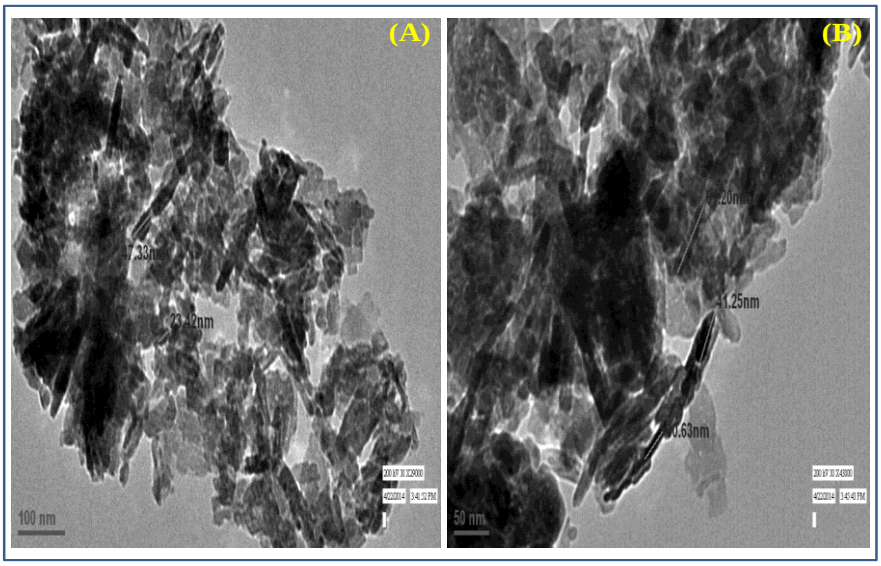


**Fig. 3.10:** TEM images of CuO nanorods

## 3.2 Structural studies

### *3.2.1 Photoluminescence (PL)*

The photoluminescence (PL) is a technique used to study the exciton spectra in conducting PANI, CuO and CuO/PANI/ITO nanocomposite. Figure depicts the comparison of emission spectra of PANI, CuO and CuO/PANI/ITO nanocomposite at the excitation wavelength 320nm, in order to certify the contribution of PANI and CuO in the nanocomposite.

The photoluminescence (PL) spectra for PANI are illustrated in figure 3.11 at excitation wavelength of 320 nm. The major peak at 360 nm and another weak peak at 376 nm are obtained. Intensity is 2390 a.u. arises due to transitions from the polaronic band to the π-band (HOMO) in structures of polyaniline. After that electron and hole pairs are recombining and the emission wavelength is shifted towards the blue. The blue shift of polyaniline demonstrates the strong quantum restriction.

In figure 12 CuO nanostructure displays photoluminescence peak at 436 nm and 456 nm. Intensity is 1740 a.u. at 320 nm excitation wavelength. It is clearly visible in the entire excitation wavelength and therefore it is assigned to the Cu vacancy level. The observed luminescence band at 436 nm is due to the recombination of relaxed excitons. But this is not due to the direct recombination of carriers into the defect levels. The peaks are related to the

crystalline defects introduced during the growth of CuO. The oxygen vacancies interact with interfacial Cu vacancies leading to the formation of a considerable amount of trapped states within the band gap, which results in a PL signal in CuO nanostructure.

PL spectra for CuO/PANI/ITO nanocomposite are illustrated in figure 3.13 at excitation wavelength 320 nm. Major peak observed at 437 nm and intensity is 6920 a.u. in case of nanocomposite red (bathochromic) shift and hyperchromic shift are observed compared to CuO and PANI.

PL wavelength and intensity is increased in nanocomposite than PANI and CuO intensity. This may be ascribed to the formation of more density of states in the energy band upon addition of CuO nanostructure in polyaniline. There are electron donating groups such as =NH in PANI, CuO is an electron conducting semiconductor, and this combination enhance the electron mobility in the nanocomposite. This in turn favors the formation of singlet exciton. The singlet exciton states so formed due to decay radiatively to the ground state resulting in enhanced photoluminescence. The relative intensity of CuO PL peak is considerably low as compared to the relative peak intensity of PANI, so it is high in the nanocomposite and it broadens the peak due to increase of the size of the particles in the nanocomposite. The increase of size of the particles in the nanocomposite is due to interaction of nanostructure of CuO and PANI. The PL study of CuO/PANI nanocomposite show that the emission peaks of PANI and CuO are presented with peak bordering and increasing intensities which confirm the increase of the size of the particles in the nanocomposite.

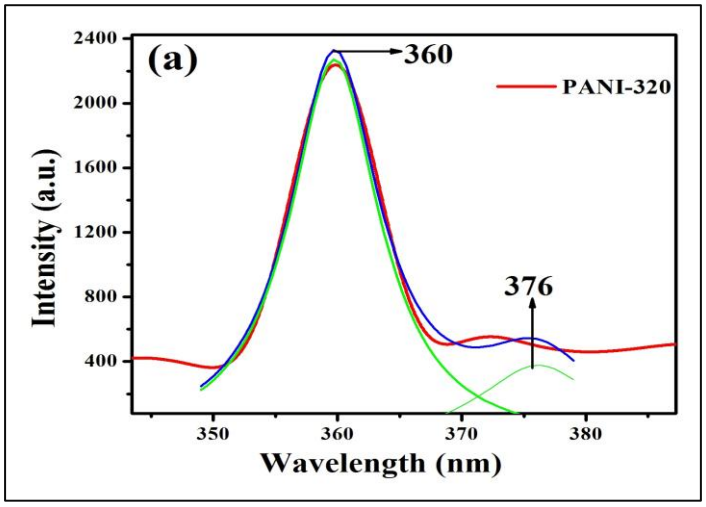


**Fig. 3.11:** PL spectra of PANI at excitation wavelength 320 nm

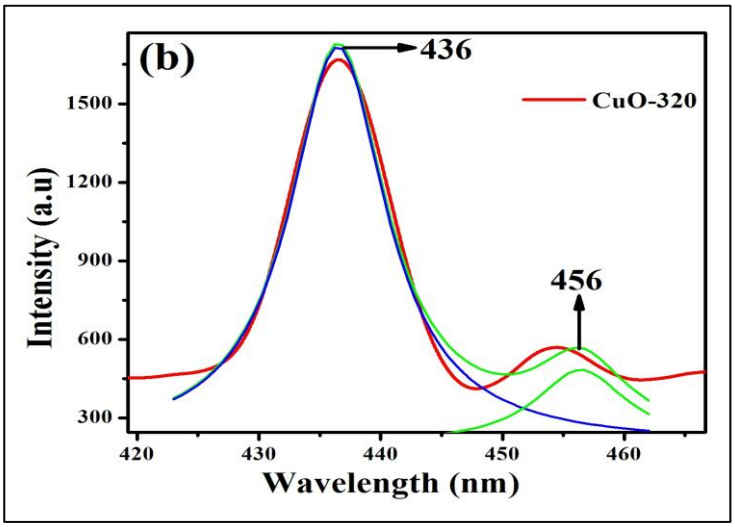


**Fig. 3.12:** PL spectra of nanostructured CuO at excitation wavelength 320 nm

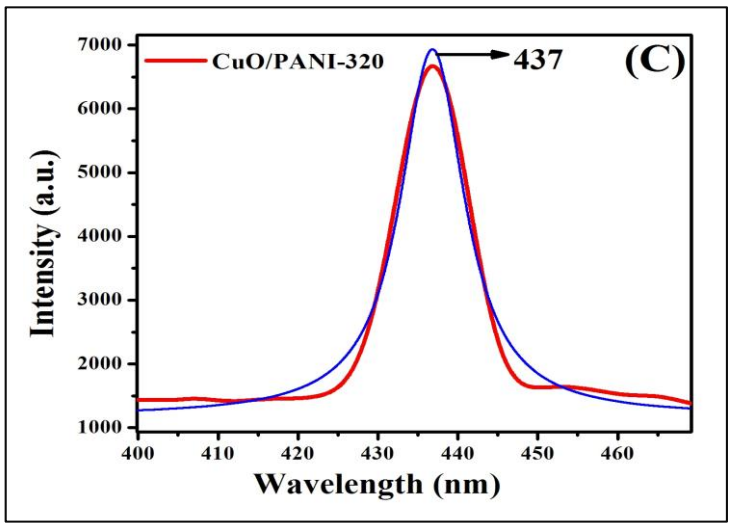


**Fig. 3.13:** PL spectra CuO/PANI nanocomposites at excitation wavelength 320 nm

### *3.2.2 UV-Visible Spectroscopy*

Figure 3.14 indicates the absorbance with respect to wavelength for PANI, CuO and CuO/PANI nanocomposite. Curve (a) instances the major absorption peaks 224, 353,440 and 595 nm and their band gap obtained 5.53, 3.51, 2.81 and 2.08 eV, respectively.

Formula for the calculate of band gap is

$$E= hc/\lambda$$

$$E=1240 \text{ eV nm}/\lambda$$

Here, h is plank constant and c is the velocity of light and λ is wavelength

The intense band 224 nm is because of π-π* transition of benzenoid ring which is connected to the extent of conjugation between the adjacent phenylene rings in the polymeric chain and the pushed planarization of π-system accelerated by collection. The less intense band at 353 nm because of π-π* transition. The peak at 440 and 595 nm is due to polaron to π* transition and transfer of electron from benzenoid ring to quinonoid ring. It contributes to enhanced conjugation and therefore lowers the band gap. This is intimately matched with the band gap of actual polyaniline (3.2-3.8 eV). The noticed bathochromic (red) shift. The π-π* transition of benzenoid ring and the establishment of polaron band in the nanocomposite are responsible for enhance of the electrical conductivity of the nanocomposite.

Curve (b) CuO nanostructure observed the major peaks at 215 nm and band gap obtained 5.76 eV.

Curve (c) shows absorption peak at 216, 264, 350 and 505 nm and band gap obtained 5.74, 4.69, 3.54 and 2.45 eV, respectively. The high intense blue shift of absorption peaks of polyaniline from its real position in the CuO/PANI/ITO nanocomposite which designates that the summation of CuO nanostructure in the polyaniline matrix has large determine on absorption spectra in the CuO/PANI/ITO nanocomposite. The high intense absorption peaks of CuO are pointed out within the nanocomposite which designates the interfacial interaction of CuO with polyaniline and this expresses the formation of polaron and bipolaron charge carrier in the nanocomposite when compared to polyaniline. The substitutions in the ring impress the tensional angle, thus dihedral/torsional angle within adjacent aromatic rings is enhanced. It causes the enhance in twisting of torsional angle which increases the band gap as compared with the band gap of PANI.

**Table 3.1:** Electronic absorption spectral data:

| PANI | | CuO | | CuO/PANI | |
|---|---|---|---|---|---|
| Absorption λmax (nm) | Band gap eV | Absorption λmax (nm) | Band gap eV | Absorption λmax (nm) | Band gap eV |
| 224 | 5.53 | 215 | 5.76 | 216 | 5.74 |
| 353 | 3.51 | | | 264 | 4.69 |
| 440 | 2.81 | | | 350 | 3.54 |
| 595 | 2.08 | | | 505 | 2.54 |
| | 3.48 | | 5.76 | | 4.12 |

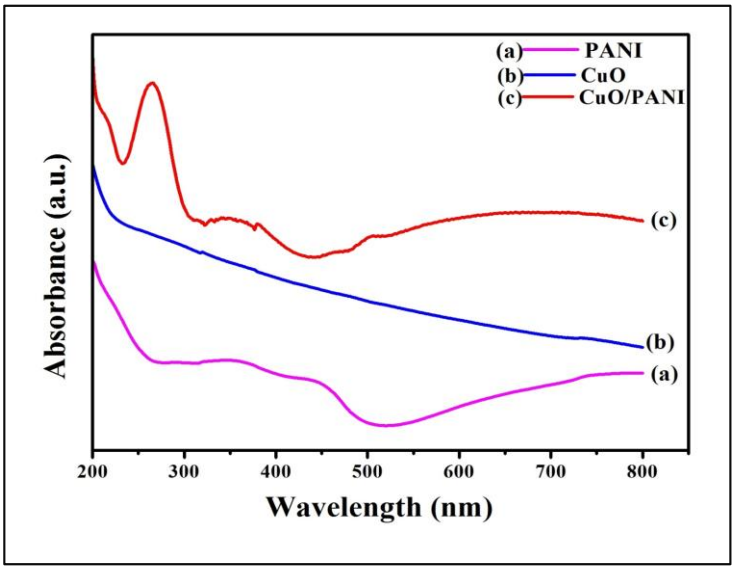


**Fig. 3.14:** Electronic absorption spectrum of (a) Polyaniline (b) CuO nanostructure (c) CuO/PANI nanocomposite

### *3.2.3 Fourier Transform Infrared Spectroscopy (FTIR)*

FTIR spectra show the chemical structure of the sample and identify the characteristic functional group

**Table 3.2:** FTIR bands ($cm^{-1}$) for PANI, CuO nanostructure and CuO/PANI nanocomposite

| **Polyaniline $cm^{-1}$** | **Copper oxide Nanoparticles $cm^{-1}$** | **CuO/PANI nanocomposite $cm^{-1}$** | **Peak assignment** |
|---|---|---|---|
| 3439 | | 3438 | N-H stretching band |
| | 3431 | | OH stretching band |
| - | - | 2924 | C-H stretching band |
| 1583 | - | 1720 | C=N stretching band |
| 1494 | - | 1639 | C=C stretching band |
| 1299 | - | 1435 | C-N stretching band |
| 1136 | - | 1107 | C-H in plane deformation |
| 813 | - | - | C-H out of plane vibration |
| - | 619 | 607 | Cu-O bending vibration |
| - | 530 | 510 | Cu-O bending vibration |

Figure 3.15 represents the FT-IR spectra of PANI, CuO and CuO/PANI nanocomposite and the peak positions related to the corresponding chemical bonds are listed in table. In case of PANI and nanocomposite bands 3439 and 3438 $cm^{-1}$ shows the N-H stretching of benzenoid ring present in the PANI and CuO/PANI nanocomposite. But in CuO nanostructures 3431 $cm^{-1}$ due to OH stretching vibration. During washing and calcinations process all hydroxide group are not removed. 1583 in PANI and 1720 in CuO/PANI nanocomposite attributed to C=N stretching mode of vibration for quinonoid units.1494 and 1639 $cm^{-1}$ corresponding PANI and CuO/PANI nanocomposite shows the C=C stretching mode of vibration for benzenoid ring. The presence of these two bands clearly shows that the polymer is composed of amine and imines units. 1299 $cm^{-1}$ in PANI and 1435 $cm^{-1}$ in nanocomposite is assigned for C-N stretching vibration. 1136 $cm^{-1}$ and 1107 $cm^{-1}$ in PANI and CuO/PANI shows the combination modes of benzenoid and quinonoid unit. Sharp peak at 814 $cm^{-1}$ is assigned to C-H out of the plane bending of the para substituted benzene rings. Two peaks 619, 530 and 607, 510 $cm^{-1}$ corresponding in PANI and CuO/PANI nanocomposite shows the presence of bending vibration of CuO crystal lattice and presence of CuO in PANI matrix.

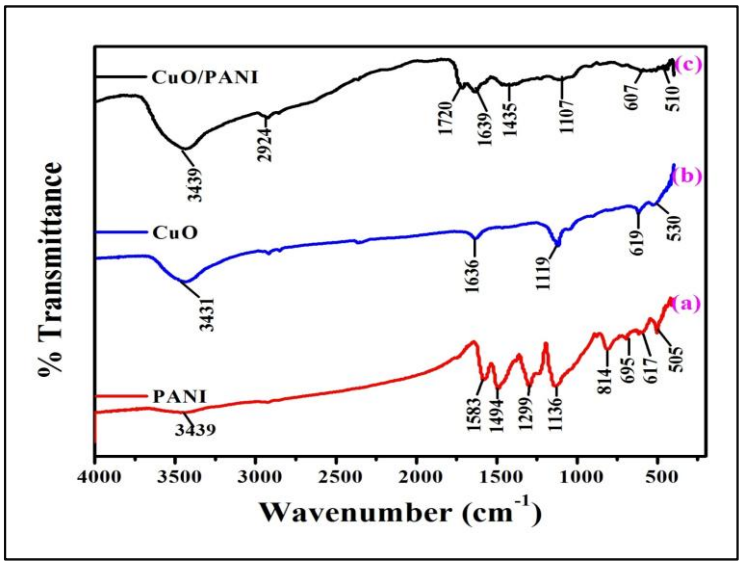


**Fig. 3.15:** Comparative FT-IR Spectrum of (a) PANI (b) CuO nanostructure and (c) CuO/PANI nanocomposite

### *3.2.4 X-ray Diffraction (XRD)*

Figure 3.16 expresses the XRD pattern of the PANI, CuO nanostructure and CuO/PANI nanocomposite, which exposes that the sample has a crystalline structure. The XRD patterns demonstrate main peaks at 2Θ= 35.62 in case of CuO nanostructure and CuO/PANI nanocomposite. That can be ascribed to the 002 reflection of CuO phase and CuO/PANI/ITO film.

Monoclinic CuO nanostructures were determined using XRD technique. Other use of XRD technique is to evaluate the particle size using Debay- Scherer equation.

Formula for the calculation of particle size are-

$$D= K\lambda/ (B\cos\Theta)$$

Where D is the mean size of crystallites (nm), K is crystallite shape factor a good approximation is 0.9, λ is x-ray wavelength its value is 1.54060 Å, B is full width at half the maximum (FWHM) in radians of the x-ray diffraction peak and Θ is the Bragg angle. In case of CuO nanostructure and CuO/PANI nanocomposite FWHM are 1.066 and 7.8 respectively. All the peaks in different pattern shows monoclinic structure of CuO, and the peaks compared with JCPDF card no- [89-5895] and miller indices (110), (002), (111), ($\bar{1}$12), ($\bar{2}$02), (020), (202), ($\bar{1}$13), (022), (220), (311) and (004) are identified. The average particle size calculated by using Debay-Scherrer formula is approximately 7.8 and 10.69 nm for CuO nanostructure and CuO/PANI nanocomposite Elastic strain calculated from XRD results it shows that below 20 nm smaller particles have high value of strain and greater the particle size have less value of strain. It clearly shows that smaller particles have high strain and bigger particles have less strain.

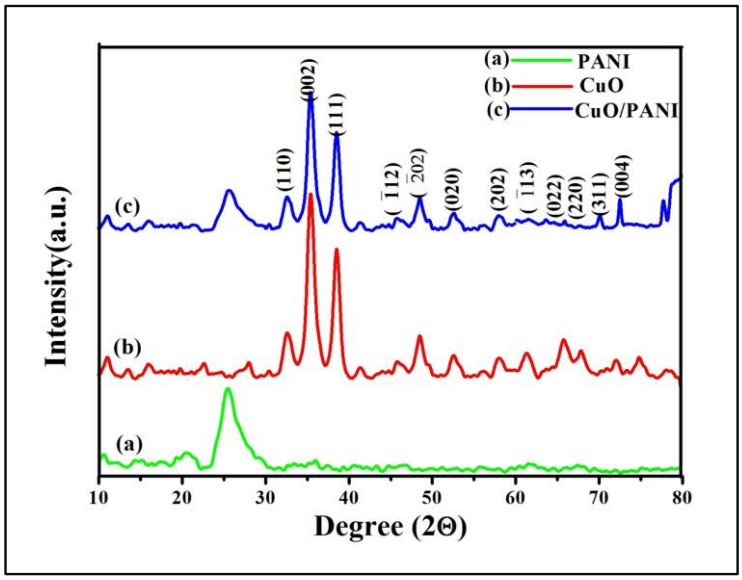


**Fig. 3.16:** XRD pattern of (a) PANI (b) CuO nanostructure and (c) CuO/PANI nanocomposite

## 3.3 Electrochemical studies

### *3.3.1 Cyclic voltammetric (CV)*

Fig.3.18 show cyclic voltammetric (CV) curve of PANI/ITO film, CuO/ITO nanostructure and PANI/CuO/ITO nanocomposite in PBS (50 mM, pH 7.5 and 0.9% NaCl) containing $[Fe(CN)_6]^{3-/4-}$ (5 mM) at a scan rate of 50mV/s. The CV of PANI, CuO and PANI/CuO bare ITO exhibits well-defined electrochemical characteristics with oxidation peak current (Ipa) 0.33, 0.49 and 0.89 mA, respectively. The oxidation potential shifts toward a higher current, and the reduction potential shifts toward a lower current. In reference to CuO/PANI/ITO electrode surface, anodic current is higher than CuO and PANI electrode. This increase is a result of the cationic and semiconducting nature of CuO and PANI respectively.

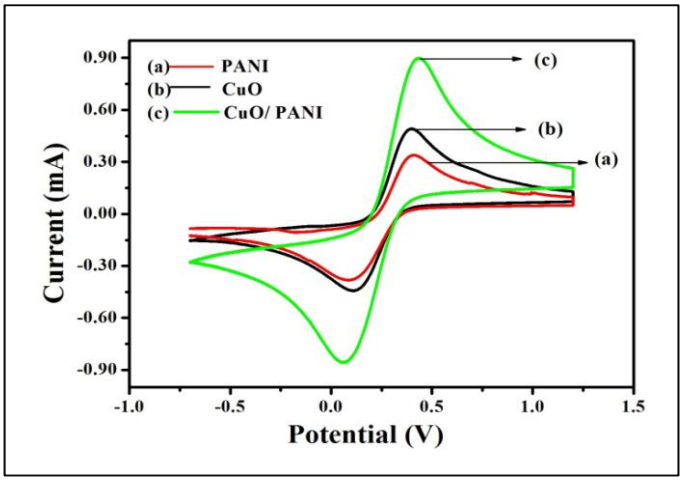


**Fig. 3.17:** Cyclic voltammogram of (a) PANI/ITO electrode, (b) CuO/ITO electrode, (c) CuO/PANI/ITO electrode

### *3.3.2 The differential pulse voltametery (DPV) studies*

Figure 3.19 show the DPV curve of PANI/ITO, CuO/ITO and PANI/CuO/ITO, having current 0.15, 0.16 and 0.19 mA and potential 0.63, 0.57 and 0.39 V, respectively. Magnitude of the peak current is higher in case of composite (CuO/PANI) than CuO nanostructure and conducting polymer (PANI). It may be due to fact that in CuO/PANI/ITO nanocomposite PANI provides an electroactive surface area that promotes electron conduction pathway and accelerated electron movement between CuO and electrode. Result in enhanced electron transfer in the interface.

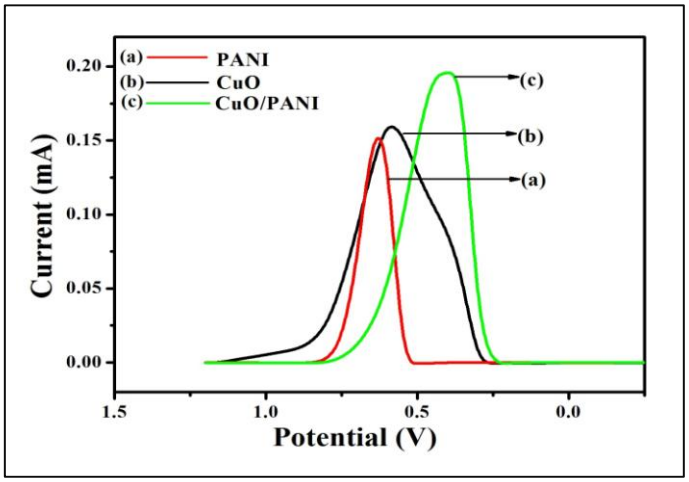


**Fig. 3.18:** DPV of the electrode (a) PANI/ITO, (b) CuO/ITO and (c) CuO/PANI/ITO.

### *3.3.3 Scan rate studies*

CV studies have been observed as a function of scan rate, was varying from 10 to 100 mV/s. The result indicates that the magnitudes of both cathodic (Ipc) and anodic (Ipa) peak currents increases linearly with the square root of scan rate. The anodic peak shifts toward more positive potential and similarly cathodic peak shifts towards more negative potential with increasing scan rate. That's showing the redox process is quasi-reversible.

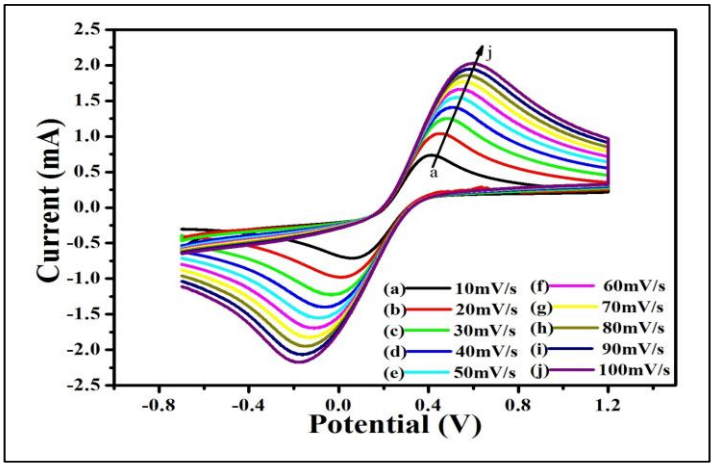


**Fig. 3.19 (A):** CV curve of the CuO/PANI/ITO electrode using an increasing scan rate of 10 to 100 mV/S

The value of electron transfer co-efficient (α), for n number of electrons, has been calculated from two straight lines with a slope equal to 2.3RT/ (1-α)nF for anodic peak and -2.3RT/α nF for cathodic peak using Laviron's equation. The electron transfer co-efficient (α) for CuO/PANI/ITO nanocomposite has been found 0.6864 V for anodic peak and 0.2771 V for cathodic peak.

The change in value of the charge transfer rate constant (Ks) of the electrode due to surface modification has been calculated by following equation

$$Ks = mnF\nu/RT$$

Where 'm' is peak to peak separation (V), n is the number of transferred electrons, F is the faraday constant (96485 $mol^{-1}$), ν is the scan rate (50mV/s), R is the gas constant (8.314 J $mol^{-1}$ $K^{-1}$) and T is the room temperature ($25^0$C). The Ks value for the CuO/ITO nanostructure and CuO/PANI/ITO nanocomposites has been found to be 585.86 $s^{-1}$ and 750.63 $s^{-1}$ respectively. Ks value increased at the surface of CuO/PANI/ITO electrode due to high catalytic behaviour of CuO nanoparticles and conducting nature of PANI. Polyaniline provide an easier path for the transfer of electrons from the redox species (CuO) and vice-versa.

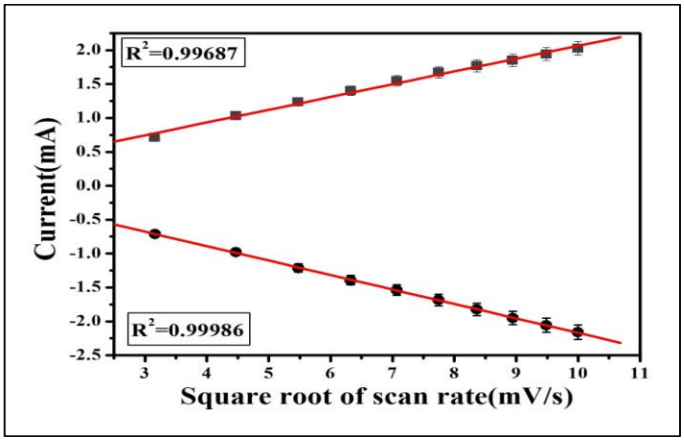


**Fig. 3.19 (B):** Magnitude of current v/s potential difference as a function of square root of scan rate (10-100mV/s)

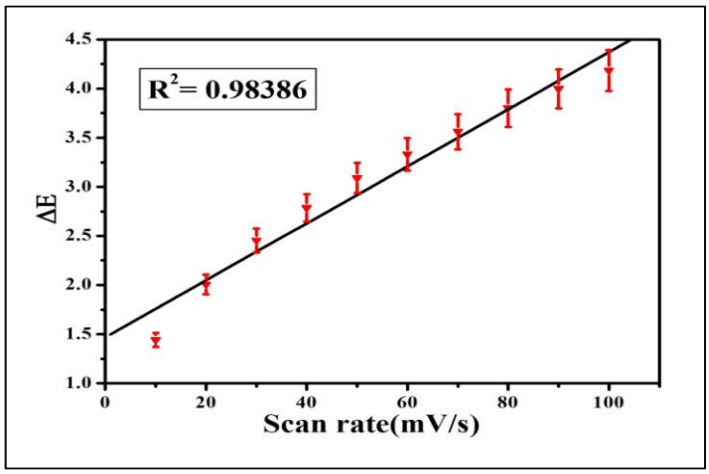


**Fig. 3.19(C):** Potential peak shift v/s scan rate

The surface concentration of the electrodes has been calculated using the Brown-Anson model by following equation

$$I_P = n^2F^2I^*A\nu/4RT$$

Where n is the number of electrons transferred, F is the Faraday constant (96485 c/mol), I* is the surface concentration of the corresponding electrode (mol $cm^{-2}$), A is the surface area of the electrode (0.25 $cm^{-2}$), ν is the scan rate (50 mV/s), R is the gas constant (8.314 J $mol^{-1}$ $K^{-1}$) and T is the room temperature ($25^0$C). The surface concentration of the CuO/PANI/ITO nanocomposite ($7.6\times10^{-8}$ mol $cm^{-2}$) is higher than that of CuO/ITO ($4.196\times10^{-8}$ mol $cm^{-2}$) electrode.

The diffusion co-efficient value (D) has been calculated for free diffusion of [Fe $(CN)_6^{3-/4-}$] from electrolyte solution to the electrode using Randles- Sevcik equation.

$$I_P = (2.69\times10^5)\, n^{3/2} AD^{1/2} C\nu^{1/2}$$

IP is the peak current, n is the number of electrons, A is the surface area of the electrode, D is the diffusion co-efficient, C is the surface concentration, ν is the scan rate (50 mV/s). D value of CuO/PANI/ITO nanocomposite is obtained as $6.173\times10^2$ $cm^2$ $s^{-1}$.

### *3.3.4 Effect of buffer pH on CuO/PANI/ITO electrode*

The effect of solution pH (5.7 to 8.0) is measured by the CV technique and observed the electrochemical behaviour of the nanocomposite (CuO/PANI/ITO) electrode in PBS (50 mM, 0.9% NaCl) containing $[Fe(CN)_6]^{3-/4-}$ (5 mM) at a 50 mV/s scan rate. It can be observed that the anodic peak current increases from pH 5.7 to 7.0 at lower potential. The highest magnitude of current is obtained at pH 7.5, further pH increases but oxidation peak current decreases and potential shifts towards higher value. These variation in peak current due to a decrease in concentration of $Cu^{+2}$ positively charged species at the matrix as the pH of PBS approaches its isoelectric point and decreases interation between redox ions and the CuO/PANI/ITO surface.

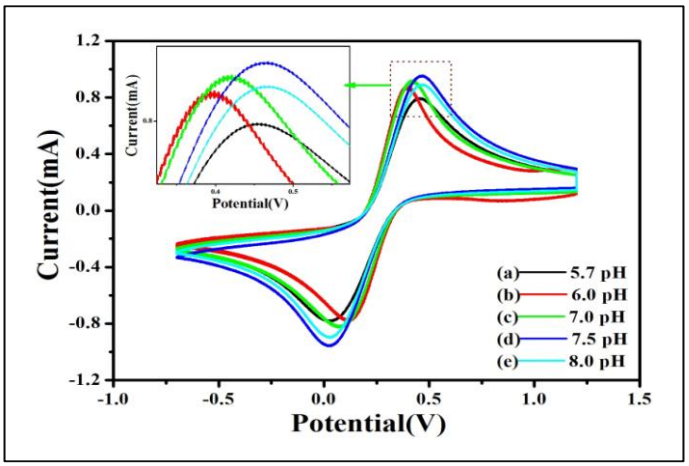


**Fig. 3.20 (A):** CV studies of the CuO/PANI/ITO electrode as a function of pH (ranging from 5.7 to 8.0) in phosphate buffer containing $[Fe(CN)_6]^{3-/4-}$

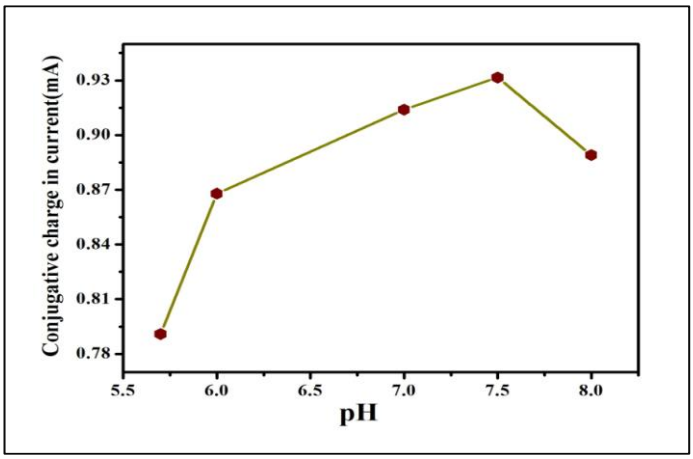


**Fig. 3.20 (B):** Changing in current as a function of pH of the PBS for the CuO/PANI/ITO electrode

### *3.3.5 Response time studies*

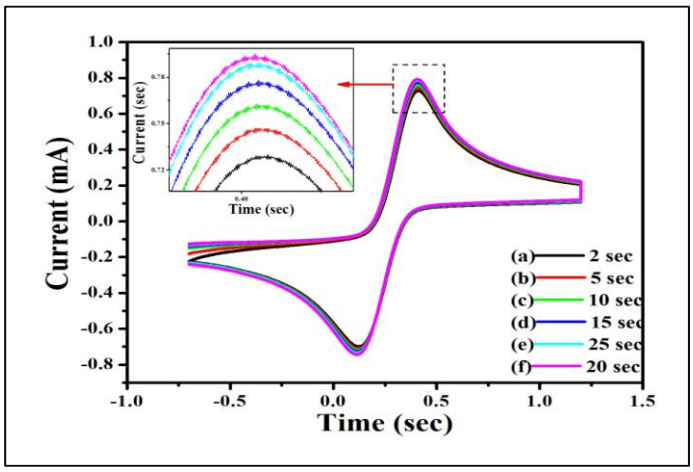


**Fig. 3.21 (A):** CV studies of the CuO/PANI/ITO electrode as a function of time (ranging from 2to 25sec) in phosphate buffer containing $[Fe(CN)_6]^{3-/4-}$

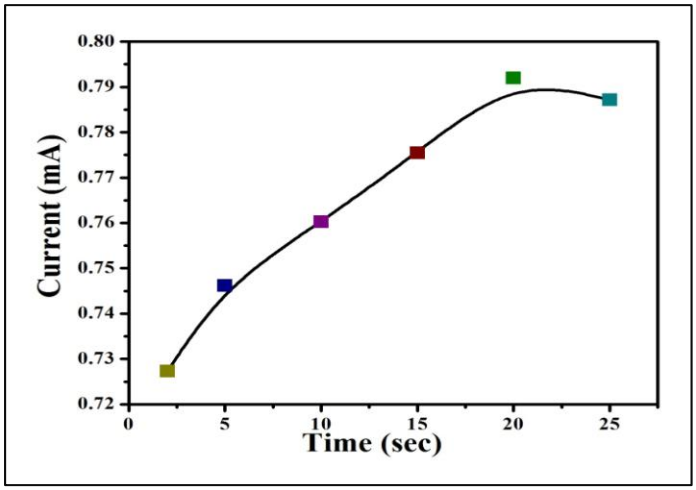


**Fig. 3.21 (B):** Electrochemical response time during the incubation period 2 to 25sec

Amperometric current response studies of the electrode show the response time of the CuO/PANI/ITO electrode has been measured at an incubation period of 2 to 25 sec. Initially, magnitude of current increases (2 to 20sec). After 20sec magnitude of current decreases, almost constant indicate that 20 sec is the response time of the CuO/PANI/ITO electrode.

### *3.3.6 Electro-catalytic study of $H_2O_2$*

The electrocatalytic behaviour of CuO/PANI was tested towards the electrocatalytic oxidation of hydrogen peroxide. Since CuO nanostructures have shown enhanced activity towards oxidation of hydrogen peroxide. The CV response of CuO/PANI/ITO electrode in phosphate buffer (pH 7.5) with changing $H_2O_2$ concentration from 0 to 22mM. The anodic peak current increases and the cathodic peak current decreases with increasing $H_2O_2$ concentration in the solution. The graph shows the calibration plot for peak current against the concentration of hydrogen peroxide. Linear calibration is obtained with a coefficient of 0.954 and 0.957 due to anodic and cathodic peak. That shows a good relation between oxidation, reduction current and concentration. The limit of detection (LOD) and sensitivity has been observed 20.7 mM and 0.0317 $\mu Mcm^{-2}$, respectively. As shown in Fig3.23 (A) the oxidation peak was observed at +0.48V v/s Ag wire when the addition of hydrogen peroxide to the electrolyte solution.

$$H_2O_2 + O_2 \longrightarrow 2H + 2e^-$$

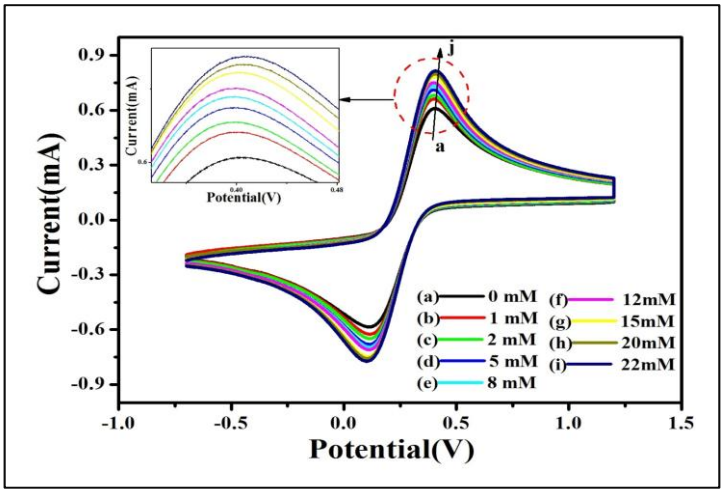


**Fig. 3.22 (A):** Electrochemical response of the CuO/PANI/ITO electrode with respect to $H_2O_2$ concentration (0mM to 22mM)

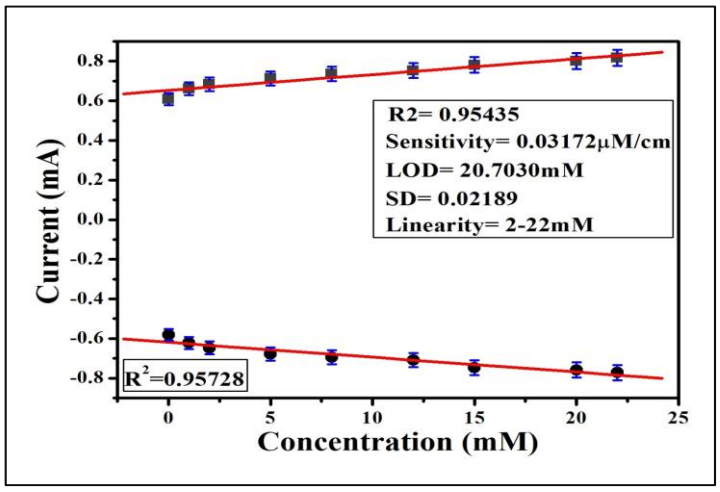


**Fig. 3.22 (B):** Calibration curve and the variation in current as a function of $H_2O_2$ concentration

### 3.4 Antibacterial activity

The antibacterial activity of the CuO nanostructure, PANI and CuO/PANI nanocomposite was tested against Gram +ve and Gram -ve bacteria that is *bacillus cereus* and *pseudomonas aeruginosa* respectively. Figure (A) shows the result after 24 h incubation of the *bacillus cereus* agar plate loaded with (I) CuO nanostructure, (II) PANI, (III) CuO/PANI nanocomposite (IV) $H_2O$. In figure [A] CuO has given a zone of inhibition of 6 mm against Gram +ve bacteria. This is attributed to the interaction between positively charged CuO and negatively charged microbial cell wall, leading to the leakage of intracellular constituents. Figure [A] PANI has a uniform bacterial growth was observed, indicating no bacterial retardation activity by PANI. Figure [A] CuO/PANI nanocomposite shows uniform bacterial growth and indicating no bacterial retardation activity. $H_2O$ do not show any bacterial retardation as $H_2O$ was taken as a control.

Figure (B) shows the result after 24 h incubation of the *Pseudomonas aeruginosa* (Gram-ve) agar plate loaded with (I) CuO nanostructure, (II) PANI, (III) CuO/PANI nanocomposite (IV) H2O. Similarly increased zone of inhibition of diameter 9 mm was observed in CuO nanostructure. And also zone of inhibition observed in (II) PANI and (III) CuO/PANI nanocomposite 5 and 1 mm, respectively.

Increased zone of inhibition (diameter) by CuO and PANI is observed in case of Gram –ve bacteria as compared to Gram +ve bacteria. This is due to difference in cell wall structure of the Gram positive and Gram negative bacteria. Hydrophilicity in Gram-ve bacteria is significantly higher than in Gram +ve bacteria, making them more sensitive to CuO and PANI.

**Table 3.3:** Zone of inhibition (mm) given by antibacterial activity of (a) CuO nanostructure, (b) PANI, (c) CuO/PANI nanocomposite (d) $H_2O$.

| Bacterial Strain | Bacterial Strain Name | Inhibition zone of various samples against bacterial Species (mm) | | | |
|---|---|---|---|---|---|
| | | (I) CuO | (II) PANI | (III) CuO/PANI | (IV) $H_2O$ used as control |
| Gram +ve | *Bacillus cereus* | 6 | - | - | - |
| Gram -ve | *Pseudomonas aeruginosa* | 9 | 5 | 1 | - |

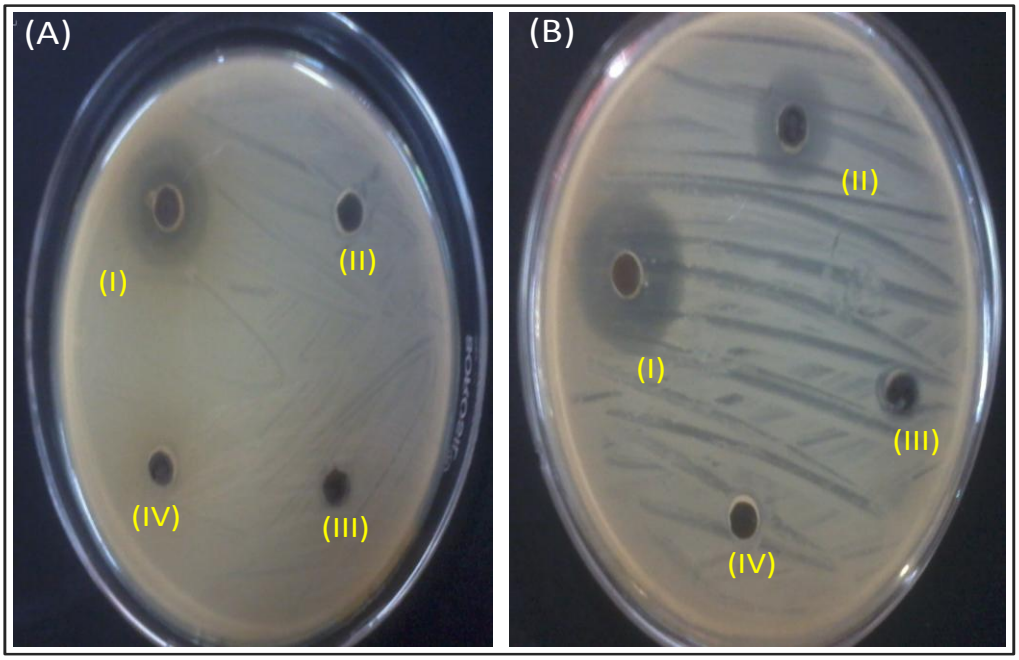


**Fig. 3.23:** Showing (A) Antibacterial activity against *Bacillus cereus* (Gram +ve) bacteria (B) Antibacterial activity against *Pseudomonas aeruginosa* (Gram -ve) bacteria where (I) CuO, (II) PANI (III) CuO/PANI nanocomposite and (IV) Water.

## 4. Conclusion and future prospects

### *4.1. Conclusions:*

We have fabricated an amperometric non enzymatic sensor by binding the CuO nanostructure (7-8 nm) with the PANI matrix. The CuO nanostructures were synthesized by sol-gel method. CuO nanostructures were dispersed in PANI solution ultrasonically and were electrophoretically deposited onto ITO surface. The CuO/PANI/ITO electrode showed rapid response (20 sec), high sensitivity 0.0317 $\mu Mcm^{-2}$, linearity (2-22 mM), standard deviation (0.02189), low detection limit (20.7 mM), good reproducibility and long term stability. The wide detection range and high sensitivity may be assigned to the amplification of the magnitude of current response since the presence of CuO nanostructures in PANI matrix and its good conducting nature improves the electron transfer between analyte (hydrogen peroxide) and CuO/PANI/ITO electrode surface. The results clearly suggest that CuO/PANI nanocomposite electrode provides an attractive matrix for impregnation of metal-oxide nanoparticles and an improved non-enzymatic sensor for the electrochemical studies.

### *4.2 Future prospects:*

Electroanalysis is a complementary technique to other analytical techniques. In this field, many of the existing analytical techniques cannot be applied as they require complex and large equipment, and so, electrochemical monitoring can bring many advantages. In the laboratory, the detection limits possible in electroanalysis make it a strong competitor for many other analytical techniques when alternatives exist. The advantage of distinguishing oxidation states is highly important. The electrochemical approach can give a rapid answer, without digestion, as to the labile fraction of a given element in a particular oxidation state, and the experiment can be performed on-site in the field. Hence recent developments are focusing on development of sensors to detect even nanometer range of materials in the environment.

Hydrogen peroxide and has found a wide range of applications in industries and medicals. In industrial application such as pulp and paper bleaching, sodium percarbonate and sodium perborate manufacturing. $H_2O_2$ is used in laundry detergents as mild bleaches; it is also used in polymerization process as flour bleaching agent. In waste water treatment $H_2O_2$ used to remove organic impurities. Sulphur based compounds present in waste is oxidized by $H_2O_2$ which is beneficial to reduce their odour. In medical application $H_2O_2$ is used as antiseptics. Chlorine based bleaches are used for the disinfection of various surfaces and recognized as antimicrobial agent. It also used for disinfecting wounds. It has low cost and ready availability compared to other antiseptics. $H_2O_2$ destroyed newly formed skin cells so very low concentration of $H_2O_2$ are used for healing and not repeatedly applied. In surgical to used for gas embolism formation. It is also used in treatment for acne. It is absorbed by skin upon contact and creates a local capillary embolism that appears as a temporary whitening of skin. In cosmetic application diluted $H_2O_2$ (3-8%) mixed with ammonium hydroxide is used to bleach human hair. Another use is to make a home- made toothpaste mixed baking soda and salt for tooth whitening. High concentrated $H_2O_2$ can be used either as oxidizer component of bipropellant rocket or as monopropellant without mixed with fuel. It decomposed into steam and oxygen when used as a monopropellant. Hydrogen peroxide also used for creating organic peroxide based explosives for examples acetone peroxide. These explosives tend to degrade quickly and hence are not used as commercial or military explosives.

However, very limited research has been done towards the sensing and electro-oxidation of hydrogen peroxide. This project work has tried to work towards this field using metal oxide-conducting polymer nanocomposite. Nanoparticles have suitable physical and chemical properties for the development of electrochemical sensors. Sensors with improved stability can be prepared using nanostructures as substrate for conducting polymer immobilization, while electrochemical sensors with improved sensitivity and selectivity can be developed making use of the catalytic properties of nanostructures.

The emergence of nanotechnology is opening new horizons for electrochemical sensors. Recent years have witnessed the development of a variety of nanomaterials based devices

exhibiting novel functions. The use of nanomaterials in such sensing devices has taken off rapidly and will surely continue to expand. Nanoparticles, nanowires and nanotubes have already made a major impact on the field of electrochemical sensors and the unique properties of nanomaterials suggest that future interdisciplinary research could lead to a new generation of electrochemical biosensors. A wide range of newly introduced nanomaterials is expected to expand the field of nanomaterials based sensors. Such nanomaterials based electrochemical devices are expected to have a major impact upon clinical diagnostics, environmental monitoring, security surveillance and food safety.

**References:**


1. R. Saini, S. Saini and S. Sharma (2010), "Nanotechnology: The Future Medicine". Journal of Cuta. and Aes. Surgery 3 (1): 32-33. DOI: 10.4103/0974- 2077.63301.
2. Nanotechnology- Wikipedia, the free encyclopedia.htm (2012).
3. R.V. Lapshin (2004), "Feature- oriented scanning methodology for probe microscopy and nanotechnology" DOI: 10.1088/0957-4484/15/9/006. ISSN 0957-4484.
4. R.V. Lapshin (2011), "Feature-oriented scanning probe microscopy" pp. 105-115. ISBN 1-58883-163-9.
5. C. Buzea, I. Pacheco and K. Robbie (2007). "Nanomaterials and Nanoparticles: Sources and Toxicity". MR 17-71. DOI: 10.1116/1.2815690. PMID 20419892.
6. A.S. Lanje, R.S. Ningthoujam, S.J. Sharma, R.K. Vasta and R.B. Pode (2010), "Int. J. Nanotechnology". 7, 979.
7. E.P. Wolhfarth (1980), "Ferromagnetic Materials", Vol. II, North-Holland, Amsterdam, New York, Oxford, Tokyo.
8. T. Mitsuyu, O. Yamakazi, K. Ohji and K.Wasa (1982), "Ferroelectrics", 42, 233.
9. O. Regan, M. Gratzel (1991), "Nature", 353, 737.
10. K. Naazeeruddin, A. Kay and M. Gratzel (1993), "J.Am. Chem. Soc.", 115, 6832.
11. U. Bjoerksten, J. Moser, M. Gratzel (1994), "Chem. Mater". 6, 858.
12. W.P. Dow, T.J. Huang (1996), "J. Catal." 160, 171.
13. P.O. Larsson, A. Andersson, R.L. Wallengerg and B. Svensson (1996), "J.Catal.", 163, 279.
14. Y. Jiang, S. Decker, C. Mohs and K.J. Klabunde (1998), "J.Catal." 180, 24.
15. H.M. Fan, L.T. Yang and W.S. Hua (2004) "Nanotechnology" 15, 37.
16. P. Poizot, S. Laruelle, S.Grugeon, L.Dupontl, J.M. Tarascon, Nature 407, 496 (2000).
17. M.K. Wu, J.R. Ashburn, C.J. Torng,P.H. Hor, R.L. Meng, L. Gao (1987), Phys. Rev. Lett 58,908.
18. V.R. Katti, A.K. Debnath, K.P. Muthe, M. Kaur, A.K. Dusa, S.C. Gadkari(2003), Sens actuators B chem , 245.
19. M.H. Chang, H.S.Liu, C.T. Tai (2011), "Powd. Tech." 207,378.
20. C.T. Hsieh, J.M. Chen, H.H. Lin, H.C. Shih (2003), Appl. Phys. Lett. 83 3383.
21. C.L. Carnes, K.J. Kalbunde (2003). J. Mol. Catal. A Chem 194,227.
22. S. Asbrink and L.J. Norrby (1970), Acta crystallogr, Sect. B: struct. Crystallogr. Cryst. Chem. 26, 8.

23. CuO crystal structure, Wikipedia.
24. J. Ying, Li, Sh. Xiong, (2009), Cryst. "Growth Des", 9 4108.
25. D. Shang, K. Yua, Y. Zhang, and Z. Zhu (2009), "Appl. Surface Sci.", 255. 4093.
26. R. Wua, Z. Maa, Z. Gua, Y. Yang (2010), "J. Alloys. Compd.", 504, 45.
27. K. Zhou, R. Wang, B. Xu, Y. Li (2006), Nanotechnology., 17, 3939.
28. N. S. Kal'chuk, P. E. Strizhak, G. R. Kosmambetova and O. Z. Didenko (2008), "Theor. Exp. Chem.", 44, 172.
29. Ch. Li, Y. Yin, H. Hou, N. Fan, F. Yuan, Y. Shi and Q. Meng (2010), "Solid State Commun.", 150, 585.
30. N. Topnani, S. Kushwaha and T. Athar (2009), "Int. J. Green Nanotechnology: Mater. Sci. Eng.", 1, 67.
31. M. Salavati-Niasari, F. Davar (2009), "Mater. Lett." 63, 441.
32. R. Vijay Kumar, R. Elgamiel, Y. Diamanty and A.G Edanken (2001), "Langmuir" 17, 1406.
33. G.G. Condorolli, G. Malandrino, I.L. Fragala (1999)."Chem. Vapour Depose". 5, 237.
34. A.A. Elseev, A.V. Lukashin, A.A. Vertegel, L.I.Heifets, A.I. Zhirov and Y.D. Treytyakov (2003), "Mater. Res Innov" 3,308.
35. D.Z. Jia, J.Q. Yu, X. Xia, Chin. Sci Bull 43,571(1998).
36. K. Brgohain, J.B. Sing, M.V.R. Rao, T.Shripathi and S. Mahumani (2000),"Phys. Rev." B 61, 11093.
37. W. S. Huang, B. D. Humphrey and A. G. MacDiarmid (1986). J. Chem. Soc., Faraday Trans. 182, 2385.
38. A. G. MacDiarmid (1997). "Synth. Met." 84, 27.
39. A. G. MacDiarmid, J. C. Chiang, M. Halpern, W. S. Huang, S. L. Mu, N. L. D.Somasiri, W. Q.Wu, S. I. Yaniger (1985). "Mol. Cryst. Liq. Cryst." 121, 173.
40. T. J. Skotheim, R. L. Elsenbaumer (1998), J. R. Reynolds. Handbook of Conducting Polymers, 2nd ed., p. 1097, Marcel Dekker, New York.
41. P. Chandrasekhar (1999). Conducting Polymers, Fundamentals and Applications: A Practical Approach, p. 760, Kluwer Academic, Boston.
42. X. Zhang and S. K. Manohar (2004). Chem. Commun. 20, 2360.
43. L. Yu, J. I. Lee, K. W. Shin, C. E. Park, R. Holze (2003). J. Appl. Polym. Sci. 88, 1550.
44. J. C. Michaelson and A. J. McEvoy (1994). Chem. Commun. 79.
45. G. C. Li and Z. K. Zhang (2004). Macromolecules 37, 2683.

46. J. M. Liu and S. C. Yang (1991). Chem. Commun. 1529.
47. W. G. Li and H. L. Wang (2004). J. Am. Chem. Soc. 126, 2278.
48. L. M. Huang, Z. B. Wang, H. T. Wang, X. L. Cheng, A. Mitra, Y. X. Yan (2002). J. Mater. Chem. 12, 388.
49. X. Zhang, W. J. Goux, S. K. Manohar (2004). J. Am. Chem. Soc. 126, 4502.
50. H. J. Qiu, M. X. Wan, B. Matthews (2001), Macromolecules 34, 675.
51. Z. X. Wei and M. X. Wan (2003). J. Appl. Polym. Sci. 87, 1297.
52. Z. X. Wei, Z. M. Zhang (2002), M. X. Wan. Langmuir 18, 917.
53. M. X. Wan (2004). "Encyclopaedia of Nanoscience and Nanotechnology", Vol. 2, H. S. Nalwa (Ed.), pp. 153–169.
54. H. J. Qiu and M. X. Wan (2001). J. Polym. Sci., Part A: Polym. Chem. 39, 3485.
55. Das, M. Dhand, C. Sumana, G. Srivastava, A. K. Nagarajan, R. Lata, N. L. Iwamoto, M. Manaka, T. Malhotra 2011. "Bio macromolecules" 12, 540−547.
56. Dhyani, H.; Ali, Md. A.; Pandey, M. K.; Malhotra (2012) J. Mater. Chem. 2012, 22, 4970−4976.
57. Y. Zhitomirsky (2002), "I. Cathodic electrophoretic deposition of ceramic and organceramic materials. Fundemental aspects. Adv. Colloid Interface Sci.", 97, 279–317.
58. V. der Biest, O. Put, S. Anné, G. Vlugels (2004), "J. Electrophoretic deposition for coatings and free standing objects. J. Mater. Sci.", 39, 779–317.
59. C. Arias, L. Cabanas-Polo, S. Gao, H. Gilabert, J. Sanchez, E. Roether, J.A. Schubert, D.W. Virtanen, S. Boccaccini (2013), "A.R. Electrophoretic deposition of nanostructured-TiO2/chitosan composite coatings on stainless steel". 3, 11247–11254.
60. A.R. Keim, S. Ma, R. Li, Y. Zhitomirsky (2010), "I. Electrophoretic deposition of biomaterials." J. R. Soc. Interface, 7, S581–S613.
61. J. Anand, S. Palaniappan, and D. N. Sathyanarayana (1998), "Conducting polyaniline blends and composites," Progress in Polymer Science, vol. 23, no. 6, and pp. 993–1018.
62. R. S. Kane, R. E. Cohen, and R. Silbey (1999), "Semiconductor nanocluster growth within polymer films," Langmuir, vol. 15, no. 1, pp. 39–43.